Review

For reprint orders, please contact: reprints@futuremedicine.com

Nanomedicine

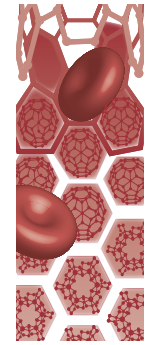

Gold nanoparticles as contrast agents in x-ray imaging and computed tomography

Lisa E Cole[1,2], Ryan D Ross[1], Jennifer MR Tilley[1], Tracy Vargo-Gogola[2,3] & Ryan K Roeder*[,1,2]

[1]Department of Aerospace & Mechanical Engineering, Bioengineering Graduate Program, 148 Multidisciplinary Research Building, University of Notre Dame, Notre Dame, IN 46556, USA

[2]Harper Cancer Research Institute, University of Notre Dame, Notre Dame, IN 46556, USA

[3]Department of Biochemistry & Molecular Biology, Indiana University Simon Cancer Center, Indiana University School of Medicine – South Bend, South Bend, IN 46617, USA

*Author for correspondence:
Tel.: +1 574 631 7003
rroeder@nd.edu

Computed tomography enables 3D anatomic imaging at a high spatial resolution, but requires delivery of an x-ray contrast agent to distinguish tissues with similar or low x-ray attenuation. Gold nanoparticles (AuNPs) have gained recent attention as an x-ray contrast agent due to exhibiting a high x-ray attenuation, nontoxicity and facile synthesis and surface functionalization for colloidal stability and targeted delivery. Potential diagnostic applications include blood pool imaging, passive targeting and active targeting, where actively targeted AuNPs could enable molecular imaging by computed tomography. This article summarizes the current state of knowledge for AuNP x-ray contrast agents within a paradigm of key structure–property–function relationships in order to provide guidance for the design of AuNP contrast agents to meet the necessary functional requirements in a particular application. Functional requirements include delivery to the site of interest (e.g., blood, tumors or microcalcifications), nontoxicity during delivery and clearance, targeting or localization at the site of interest and contrast enhancement for the site of interest compared with surrounding tissues. Design is achieved by strategically controlling structural characteristics (composition, mass concentration, size, shape and surface functionalization) for optimized properties and functional performance. Examples from the literature are used to highlight current design trade-offs that exist between the different functional requirements.

Keywords: computed tomography • contrast agent • delivery • gold nanoparticles • surface functionalization • targeting • x-ray imaging

Background

X-ray imaging & computed tomography

After Wilhelm C Roentgen discovered x-ray radiation in 1895, x-ray imaging rapidly became an important clinical diagnostic tool, enabling noninvasive visualization inside the human body [1]. Today, x-ray imaging, including computed tomography (CT), accounts for 75% of all clinical diagnostic imaging [1] due to providing relatively inexpensive, high-resolution imaging. The introduction of CT in 1972 enabled 3D anatomic reconstructions instead of 2D projected images or planar radiographs, in which important details could be obscured due to shadowing or overlapping structures [2]. CT has become widely utilized in clinical diagnostic imaging, with an estimated 70 million CT scans performed annually in the USA [3], and is considered the most important discovery in diagnostic x-ray imaging since the discovery of x-rays [4]. Continued incremental improvements to CT have included: spiral CT in the late 1980s, which improved spatial resolution; multislice imaging in the early 2000s, which decreased scan time; helical cone-beam CT technologies, which are currently emerging for rapid scanning at high spatial resolution; and the continuous development of new reconstruction algorithms for handling the scanning patterns associated with helical or cone-beam

Future Medicine part of fsg

CT [4,5]. Current developments include the clinical introduction of dual-energy CT [6] and research into spectral (color) CT [7,8].

CT exhibits higher spatial and temporal resolution [9], but lower sensitivity [10] compared with other clinical imaging modalities, such as PET and MRI. In addition, CT has lower associated costs and is more widely available than MRI. Image contrast in CT is derived from differences in the x-ray attenuation of tissues. However, the ability to distinguish between neighboring tissues can be problematic due to subtle differences in the x-ray attenuation of many soft tissues, which results in a low signal-to-noise ratio. The signal-to-noise ratio can be increased at lower x-ray energies, but not without an increased radiation dose and potential health risks for patients [11]. Thus, an inherent trade-off exists between image sensitivity (or contrast) and radiation dose.

Contrast agents for CT

X-ray contrast agents were introduced in order to enhance the contrast between tissues with similar and/or low x-ray attenuation by increasing the signal-to-noise ratio without increasing the radiation dose to the patient. X-ray contrast agents used clinically include barium sulfate suspensions and iodinated molecules. Barium sulfate was first introduced as a clinical contrast agent in 1910 [1] and is currently used for gastrointestinal imaging after oral administration [12]. Barium sulfate suspensions are relatively inexpensive and routinely used in an estimated 5 million x-ray procedures per year in the USA [1]. Thus, barium sulfate contrast agents are a mature technology and are not presently an active area of research.

Iodinated molecules were first used as a contrast agent in 1923 [13] and have undergone significant improvements since then. The first water-soluble contrast agents utilized sodium iodide, which was toxic at the concentrations necessary for imaging contrast. Current agents are most commonly low-molecular-weight iodinated aromatics, which are highly water soluble and exhibit low toxicity [14]. Active targeting has been enabled by the conjugation of functional ligands onto the aromatic rings [15]. Iodinated molecules are most commonly used as vascular contrast agents. However, iodinated contrast agents exhibit a relatively short blood circulation time and rapid clearance through the kidneys, leading to a short imaging window, which may require multiple injections. A recent clinical report associated sudden exposure to high levels of iodinated contrast agents with a risk of developing thyroid dysfunction [16], although further investigation is necessary to determine a casual relationship and the general population risk.

Gold nanoparticles as x-ray contrast agents

Over the last decade, gold nanoparticles (AuNPs) have gained attention as an x-ray contrast agent following initial reports by Hainfeld *et al.* in 2004 and 2006 [17,18]. Subsequent research and clinical interest, as gauged by the annual number of publications on AuNPs as x-ray contrast agents, have grown steadily due to a number of favorable properties of AuNPs. Gold exhibits a relatively high x-ray attenuation coefficient compared with both barium sulfate and iodine, especially at the energy levels used for clinical CT [19]. Furthermore, AuNPs exhibit a longer vascular retention time compared with iodinated molecules, due to their higher molecular weight, which potentially increases the available imaging window [18]. AuNPs are readily surface functionalized for enhanced colloidal stability and/or targeted delivery. In fact, a sharp increase in the annual number of research publications on AuNPs as x-ray contrast agents occurred in 2010, when several groups demonstrated active targeting *in vivo* with surface-functionalized AuNPs, which could enable molecular imaging capabilities with CT [20–23].

Investigations of AuNPs as an x-ray contrast agent can be categorized by three potential applications in diagnostic imaging [24]: blood pool, passive targeting and active targeting (Figure 1). Blood pool contrast agents are designed to remain in the bloodstream for a prolonged amount of time by limiting diffusion through the vascular endothelium [25] in order to enable a longer imaging window [15]. Passive targeting relies on the nonspecific accumulation of AuNPs within a site of interest by leveraging the enhanced permeability and retention effect, in which appropriately sized molecules or nanoparticles accumulate more readily in tumor tissues compared with normal surrounding tissues [26,27]. Tumor vasculature is described as 'leaky' due to a distortion of the endothelial layer of blood vessels, allowing AuNPs to escape the vasculature and enter the tumor microenvironment. Active targeting is the ability to deliver and retain a contrast agent at a specific site of interest through surface functionalization with molecules, such as peptides or antibodies, which exhibit a specific affinity for that site [26,27]. AuNPs have been targeted to cancer cells and tumors by exploiting the overexpression of a number of receptors on cancer cells compared with normal cells.

Design of AuNPs as x-ray contrast agents

AuNPs must be designed to meet the necessary functional requirements for a contrast agent in a particular clinical or preclinical application. These functional requirements include (Figure 2):

Delivery: "Go where we want." The contrast agent must be able to be delivered *in vivo* and transported to the site of interest.

Nontoxic: "Do no harm along the way." The contrast agent must not cause adverse side effects to organs during delivery and clearance.

Targeting or localization: "Stay where we want." The contrast agent must accumulate and be retained at site(s) of interest (e.g., blood pool, tumor or microcalcification, among others).

Contrast enhancement: "Show what we want." The contrast agent must increase the x-ray attenuation of the site of interest compared with surrounding tissues.

These functional requirements can be achieved by designing nanoparticles to have specific properties through control over structural characteristics (Figure 3). Key properties include the x-ray attenuation coefficient, colloidal stability in physiological media and during storage, vascular retention time, biodistribution and cytotoxicity. These physical, colloidal and biological properties are governed by structural characteristics, including the nanoparticle composition, mass concentration, size, morphology and molecular functional groups. Similar structural characteristics have been put forward as critical design parameters in other reviews for a variety of hard and soft nanoparticles [28,29]. Thus, design is achieved by strategically controlling these structural characteristics for optimized properties and functional performance, such that clinical efficacy is a product of engineering design.

The overall goal of this article is to summarize the current state of knowledge regarding AuNP x-ray contrast agents within a paradigm of key structure–property–function relationships (Figure 3) in order to provide guidance for the design of AuNP contrast agents to meet the necessary functional requirements in a particular clinical or preclinical application. Therefore, this article is organized by the structural characteristics that can be tailored to meet functional performance requirements (Figures 2 & 3). Examples from the literature are used to highlight current design trade-offs that exist between the different functional requirements. Note that while this article focuses exclusively on AuNPs as x-ray contrast agents, nearly all of the key structure–property–function relationships and design trade-offs similarly apply to other nanoparticle x-ray contrast agents [1,12,14,25].

Composition

The composition of an x-ray contrast agent directly affects the number of x-rays that can be attenuated and therefore the ability to enhance contrast. The x-ray attenuation of a contrast agent is dependent on the atomic number, bulk density, x-ray source energy spectrum and presence or location of x-ray absorption edges.

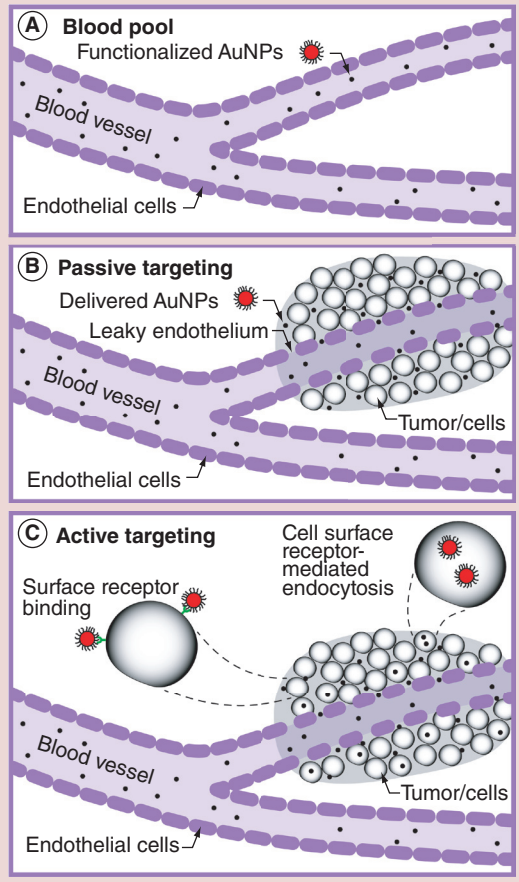

Figure 1. Three applications for the use of gold nanoparticles as x-ray contrast agents in diagnostic imaging. (A) Blood pool, **(B)** passive targeting and **(C)** active targeting. Blood pool retention is achieved by limiting diffusion through the vascular endothelium, while passive targeting is promoted by transport across the 'leaky' endothelium present in tumors. Passive targeting is nonspecific, while active targeting is achieved by specific binding interactions between cell surface receptors and molecules, such as peptides or antibodies, attached to AuNP surfaces.
AuNP: Gold nanoparticle.

Contrast-enhancement

X-ray imaging is based on the absorption or scattering of photons as a collimated x-ray beam passes through a specimen. As x-ray photons are absorbed or scattered, the intensity (I) of the x-ray beam is reduced as:

$$I = I_o e^{-x\mu/\rho}$$

where I_o is the initial intensity of the x-ray beam, x is the thickness of the specimen, μ is the linear x-ray attenuation coefficient (cm^{-1}) of the specimen material or tissue and ρ is the material or tissue bulk density (g/cm^3). In CT, x-ray attenuation is measured in Hounsfield

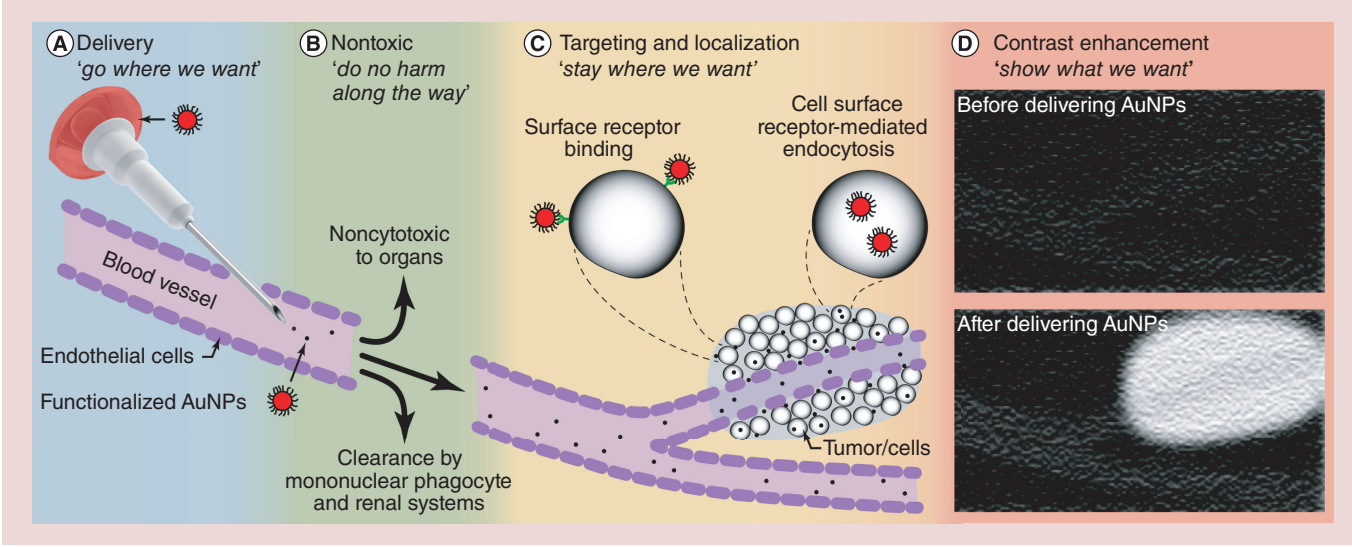

Figure 2. Schematic diagram (not to scale) showing the necessary functional requirements for gold nanoparticle x-ray contrast agents: delivery, nontoxic, targeting and localization and contrast enhancement. **(A)** The contrast agent must 'go where we want'; it must be able to be delivered *in vivo* and transported to the site of interest. **(B)** The contrast agent must 'do not harm along the way'; it must not cause adverse side effects to organs during delivery and clearance. **(C)** The contrast agent must 'stay where we want'; it must accumulate and be retained at site(s) of interest (e.g., tumor). **(D)** The contrast agent must 'show what we want'; it must increase the x-ray attenuation of the site of interest compared with surrounding tissues.
AuNP: Gold nanoparticle.

units (HU) by calibration with water (0 HU) and air (-1000 HU) as:

$$HU = \frac{\mu - \mu_{water}}{\mu_{water}} \cdot 100$$

where μ is the linear x-ray attenuation coefficient of the material or tissue and μ_{water} is the linear x-ray attenuation coefficient of water. Image contrast is derived from differences in the linear x-ray attenuation coefficient and the thickness of two neighboring materials or tissues (e.g., muscle and bone, where bone attenuates a proportionally greater number of x-rays, leading to a greater degree of incident intensity reduction, or greater x-ray attenuation). Materials or tissues with high atomic number (Z) and bulk density (ρ) generally absorb more x-rays. Therefore, high atomic number elements, such as barium, iodine or gold, exhibit a high mass attenuation coefficient (μ/ρ), and are thus good candidates for x-ray contrast agents in soft tissues (Figure 4). Gold (Z = 79) has a higher atomic number compared with iodine (Z = 53) or barium (Z = 56) and can thus absorb more x-rays at specific energy levels (Figure 4).

X-ray attenuation is also dependent on the x-ray photon energy, which governs the initial intensity (I_o) and also independently influences the x-ray attenuation coefficient. The mass attenuation coefficient is decreased as incident photon energy from the x-ray source is increased (Figures 4 & 5). Differences in the x-ray attenuation coefficient between two different materials are therefore greater at lower tube potentials (Figure 4), but the radiation dose is also greater [11]. The incident x-ray photon energy spectrum is controlled by setting the peak tube potential (kVp), which corresponds to the maximum photon energy in the beam. For example, a 100 kVp tube potential results in a spectrum of tube potentials below 100 keV. Beam filtration is used to tune the energy spectrum by limiting the number of low-energy photons (<15 keV), and also high-energy photons in mammography, using a filter material (commonly aluminum, copper or molybdenum, among others). Therefore, the peak tube potential range is typically 25–35 kVp in mammography [30], 50–80 kVp in clinical radiography [31] and 80–150 kVp in clinical CT [14] in order to achieve sufficient contrast while minimizing the radiation dose. The high x-ray attenuation coefficient of gold compared with both iodine and barium within these energy ranges (Figure 4) suggests that gold can enable improved contrast enhancement [19].

The mass attenuation coefficient also exhibits a step increase, called an 'absorption edge', when incident x-ray photons possess a greater energy than the binding energy of the inner-shell electrons of an element in the material, such that an electron is ejected and the vacancy filled by an outer-shell electron. At the photon energy levels utilized in CT and other x-ray imaging systems, *K*-shell electrons may be ejected, resulting in a *K*-edge (Figure 4). The *K*-edges for iodine, barium and gold are located at 33.2, 37.4 and 80.7 keV, respectively

[19]. Thus, the contribution of absorption edges to x-ray attenuation is greatest when the mean energy of the source spectrum is near the contrast agent *K*-edge. Moreover, absorption edge subtraction can be used to increase the signal-to-noise ratio by subtracting images taken at energy levels above and below the *K*-edge of a material or contrast agent [33].

A number of phantom studies have demonstrated that AuNPs enabled greater contrast per unit mass compared with iodine at various energy levels [20,34–41], as expected due to the higher atomic number and x-ray attenuation coefficient of gold. For example, at 100 keV, gold enables 2.7-times greater contrast per unit mass compared with iodine [18]. However, differences in the x-ray source energy spectrum result in significant differences in the apparent improved contrast of gold versus iodine due to the different locations of the *K*-edges for gold (80.7 keV) and iodine (33.2 keV) [39,41]. Thus, direct study-to-study or quantitative comparisons are only possible using the same imaging system or x-ray source spectra. For example, at moderate tube potentials (70–90 kVp), there was no detectable difference between AuNPs and iodine at equal mass concentrations, but AuNPs provided significantly greater x-ray attenuation compared with iodine at low (40–60 kVp) and high (100–140 kVp) tube potentials [39], which are clinically relevant ranges for mammography or planar radiography and CT, respectively. Therefore, experiments aimed at comparing AuNPs with clinically available iodine contrast solutions, or any other contrast agent, must consider the resultant x-ray energy spectra produced by an imaging system at a specific tube potential (kVp) relative to contrast agent absorption edges.

AuNPs have also been compared with iodine *in vivo* in blood pool imaging [40,42] and passive targeting of a tumor [18]. AuNPs enabled greater vascular and tumor contrast compared with iodine at each imaging time point in each study after administering an equal-mass dose of gold and iodine. Therefore, AuNPs provided greater contrast compared with iodine *in vivo,* demonstrating the clinical potential of AuNPs as an x-ray contrast agent. However, the greater contrast provided by AuNPs compared with iodine in these *in vivo* studies was not likely only due to compositional differences in x-ray attenuation, but also differences in the mass concentrations of gold or iodine that were able to be delivered and retained at the site of interest.

Mass concentration

At the photon energy ranges used in radiography and CT (10–140 keV), the x-ray attenuation of high atomic number elements is primarily governed by photoelectric absorption due to differences in mass concentration [19,43–44]. A greater mass concentration will lead to greater x-ray attenuation; therefore, the delivery of a larger mass payload to the site of interest will increase the contrast enhancement. However, large doses of exogenous contrast media may cause adverse side effects *in vivo*, including toxicity. Therefore, an appropriate dose must be determined in order to enhance contrast without inducing cytotoxicity. One of the main limitations of CT compared with other imaging modalities is the relatively high mass concentration of contrast agent necessary for contrast-enhanced imaging. CT typically requires millimolar concentrations, while MRI can detect micromolar concentrations [12,45].

Contrast enhancement

Phantom studies have shown that the x-ray attenuation of AuNPs increases linearly with mass concentration [22,32,34–36,41,46–48], indicating that the delivery of a greater mass concentration to the site of interest will enable greater contrast enhancement (Figures 5 & 6A). A differential contrast (ΔHU) of at least 30 HU has been suggested to be necessary for visibly apparent contrast enhancement in clinical CT [49]. The minimum detectable mass fraction of a contrast agent within a given matrix can be calculated by the change in the mass attenuation coefficient per change in the mass fraction of the contrast agent [50]. Thus, a matrix with a high background x-ray attenuation (e.g., bone)

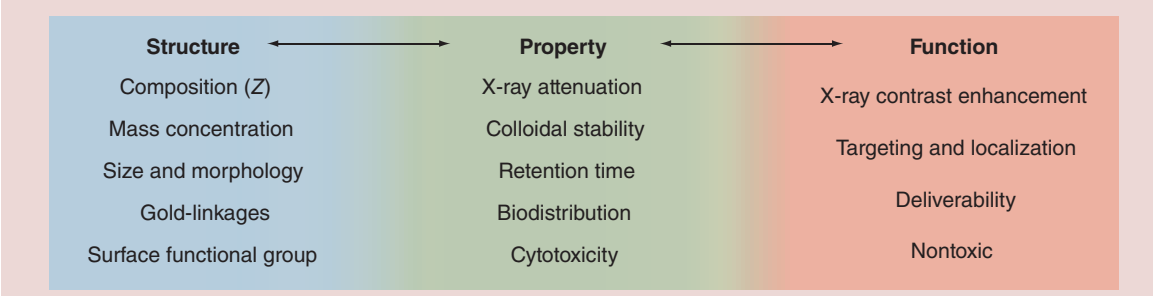

Figure 3. Key structure–property–function relationships to guide the design of gold nanoparticles as x-ray contrast agents for a particular clinical or preclinical application.
Z: Atomic number

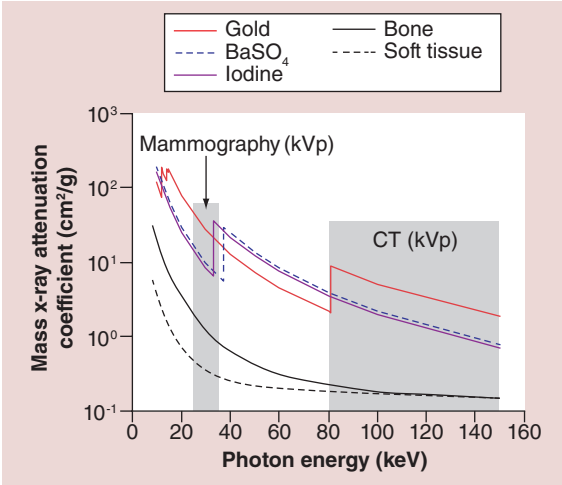

Figure 4. Energy-dependent differences in the mass x-ray attenuation coefficient (μ/ρ) of gold compared with current clinical contrast agents ($BaSO_4$ and iodine) and tissues. The peak tube potential (kVp) used in clinical mammography and CT systems is shown (gray shading) to highlight the potential advantage of gold nanoparticles due to exhibiting a greater x-ray attenuation compared with both barium sulfate and iodine at the energy levels used for clinical imaging. Note the presence of a *K*-shell absorption edge for iodine, barium and gold at 33.4, 37.4 and 80.7 keV, respectively.
$BaSO_4$: Barium sulfate; CT: Computed tomography.
Data taken from [19].

will require a higher mass fraction of gold for the same increase in contrast compared with a low-attenuating background (e.g., a tumor). Specifically, assuming that a differential contrast of 30 HU is necessary for detection at 80 keV, the mass concentration of AuNPs delivered to bone would need to be 0.34 versus 0.18 wt% delivered to soft tissue. Therefore, the dose of AuNPs necessary for contrast enhancement may differ greatly depending on the background signal at the site of interest.

Deliverability & targeting

The delivery of a high mass concentration of AuNPs to a site of interest enables greater contrast, due to the linear relationship between mass concentration and x-ray attenuation (Figures 5 & 6A) described above, but is not guaranteed simply by increasing the initial dose of AuNPs. A number of factors impact the delivery of a sufficient mass concentration for x-ray imaging, including the surface chemistry of AuNPs and the targeted site of interest.

In vitro cell labeling studies demonstrated that the mass concentration of nontargeted AuNPs internalized by cells increased with the initial mass concentration or dose of AuNPs, but a saturation point was reached (Figure 6B & Table 1) [36,51]. Nonspecific adsorption of proteins on the surface of citrate-stabilized AuNPs was demonstrated to facilitate uptake of AuNPs in cells through a receptor-mediated endocytosis pathway [51]. This mechanism depends not only on the number of AuNPs, but also the density of active receptors on the cell membrane [52]. Therefore, once the number of active receptors is saturated, a further increase in the dose of AuNPs no longer facilitates an increase in the mass concentration delivered and thus x-ray attenuation (Figure 6). A saturation point in the cellular uptake of nontargeted AuNPs also appears be dependent on the AuNP size [53] and surface chemistry [54], as well as the cell line and specific culture conditions [55,56]. Therefore, dosing studies are important for evaluating the functional performance of a given AuNP formulation within a given model system [53].

The delivery of actively targeted AuNPs is even more complex and the mass concentration of delivered AuNPs further depends on the binding affinity of the targeting molecule and the prevalence of receptor or binding sites available on the cell, tissue or other substrate [62]. *In vitro* cell labeling studies demonstrated that cells positive for the targeted receptor were able to internalize a greater mass of AuNPs compared with cells without the receptor or when treated with nontargeted AuNPs [47–48,61,63–72]. AuNPs targeted to mineral surfaces were shown to reach a saturation point in the surface density of AuNPs labeling mineral surfaces *in vitro* [32,73], similar to the saturation point observed for the nontargeted delivery of AuNPs to cells. Whether or not a similar saturation point exists for the targeted delivery of AuNPs to cells does not yet appear to be known.

Understanding the effects of the initial dose is particularly important *in vivo,* as the initial dose not only affects the mass concentration delivered to the site of interest and resultant contrast enhancement, but also the mass concentration of AuNPs accumulated in other organs. In fact, one study has shown that the mass concentration of AuNPs in blood did not increase as the concentration of the administered dose increased, but the mass accumulated in other organs did increase proportionally to the administered dose [74], which could be problematic for blood pool imaging applications. This adds further weight to the importance of dosing studies to determine the minimum effective dose for x-ray imaging.

Toxicity

Although a high mass concentration at the site of interest may be desired for contrast enhancement, the required dose of AuNPs could result in toxicity or other adverse side effects. In general, AuNPs are considered to be nontoxic based on a multitude of *in vitro* and *in vivo* studies, which are reviewed elsewhere [55,56]. In particular, studies investigating AuNPs as an x-ray con-

trast agent have shown AuNPs to be nontoxic *in vitro* at concentrations up to 500 mM (~98.5 mg/ml) [20] and *in vivo* at doses up to 2700 mg/kg (Figure 7) [17,18]. However, it should be noted that very small AuNPs (1.9 nm) were used at the highest *in vivo* dose and were rapidly cleared by the kidneys [17,18]. AuNPs larger than 1.9 nm were shown to be nontoxic *in vivo* at doses ranging from 79 to 500 mg/kg while enabling successful contrast-enhanced imaging (Table 2).

Despite broad consensus on the low cytotoxicity of AuNPs *in vitro*, a few less favorable reports in the literature give pause for caution. For example, AuNPs were shown to alter the *in vitro* cell morphology of human dermal fibroblasts at a concentration of 0.4 mM (~0.08 mg/ml) [75]. Changes in the cellular cytoskeleton could impact cell proliferation, migration and adhesion. In addition, the number of cells undergoing apoptosis were reported to increase with increased AuNP concentration *in vitro* [76]. Whether these reports are outliers or causes for concern is not yet known. In a thorough review on the topic, Khlebtsov *et al.* [55] suggested that AuNPs are nontoxic *in vitro* as long as the concentration of AuNPs is below 10^{12} particles/ml, which corresponds to approximately 0.05 mM (~0.01 mg/ml) for 10 nm AuNPs, approximately0.8 mM (~0.16 mg/ml) for 25 nm AuNPs, approximately 6.4 mM (~1.3 mg/ml) for 50 nm AuNPs, approximately 21.6 mM (~4.3 mg/ml) for 75 nm AuNPs and approximately 51.3 mM (~10.1 mg/ml) for 100 nm AuNPs (Figure 7).

In vivo cytotoxicity has not been rigorously evaluated within studies focused on the use of AuNPs as x-ray contrast agents. General investigations into the *in vivo* cytotoxicity of AuNPs have reported responses ranging from no evidence of toxicity [74,77], to minor liver inflammation [78,79] to noticeable weight loss and early death in mice [80], all at doses below the range utilized in studies investigating AuNPs as an x-ray contrast agent (Figure 7). The varied responses suggest that the administered dose may not be the only factor determining the *in vivo* toxicity of AuNPs. There is evidence that the delivery route can also impact toxicity: oral and intraperitoneal delivery were reported to result in higher toxicity compared with intravascular delivery [77]. Furthermore, the AuNP size and surface chemistry may also directly affect the delivery of the administered dose and the *in vivo* performance of AuNPs, as discussed below.

Size & morphology

AuNPs of varying size and shape can be readily synthesized using various methods, which are reviewed in detail elsewhere [81]. Therefore, AuNPs spanning a wide range of sizes and shapes have been investigated as x-ray contrast agents, heightening the importance of fundamental understanding for the effects of AuNP size and shape on functional performance.

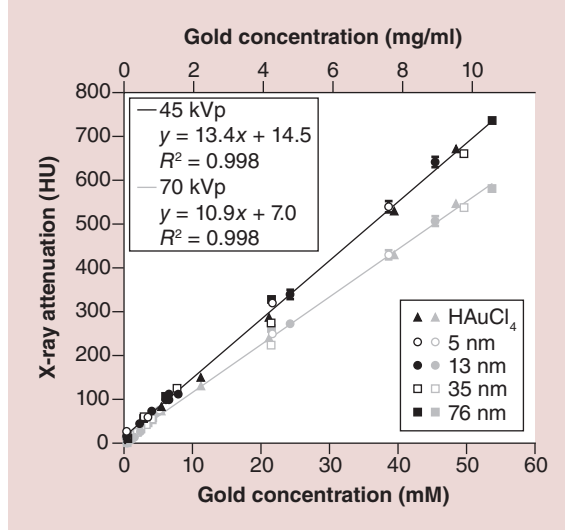

Figure 5. Mean linear attenuation coefficient (μ) in Hounsfield units (HU) measured by micro-computed tomography at 45 and 70 kVp for chloroauric acid ($HAuCl_4$) and gold nanoparticles with a mean diameter of 5, 13, 35 and 76 nm dispersed in distilled water at gold concentrations ranging from 0 to 54 mM (~0 to 10.6 mg/ml). Error bars show one standard deviation of the mean (n = 5 per data point). Error bars that are not shown lie within the data point. The x-ray attenuation of gold nanoparticles imaged at 45 kVp was significantly greater than the x-ray attenuation of the same gold nanoparticles imaged at 70 kVp ($p < 0.0001$, generalized linear model), as expected. However, the x-ray attenuation was not influenced by gold nanoparticle size ($p > 0.85$, generalized linear model).
$HAuCl_4$: Chloroauric acid; HU: Hounsfield unit.
Data taken from [32].

Contrast enhancement

The size and morphology of AuNPs is well known to influence the absorption and scattering of visible light [82,83], which likely enticed researchers to investigate similar effects on x-ray absorption and scattering, but no such effect exists for x-ray imaging. Initial reports presented conflicting data, with one showing that the x-ray attenuation exhibited by smaller AuNPs (4 nm) was greater than larger particles (20, 40 and 60 nm) at the same concentration [36], and another showing no difference in x-ray attenuation between AuNPs of various sizes or shapes (spheres of ~4, 6 and 25 nm, and rods of ~30 nm diameter and ~63 nm length) [84]. However, a recent report proved that x-ray attenuation is not influenced by AuNP size [32] by directly comparing the x-ray attenuation of AuNPs over a wide range of mean particle diameters (5, 13, 35 and 76 nm), including aqueous solutions of chloroauric acid com-

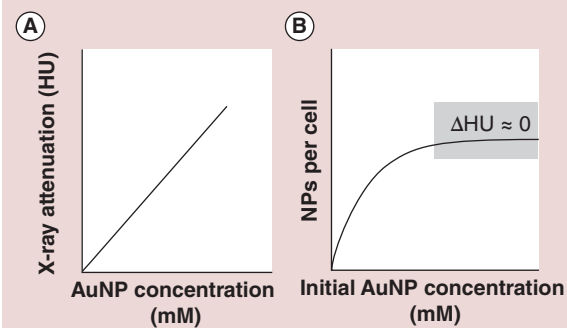

Figure 6. Schematic diagram showing critical effects of the mass concentration of gold nanoparticles on contrast enhancement and passive delivery to cells.
(A) X-ray attenuation increases linearly with an increase in the mass concentration of AuNPs, as demonstrated in a number of imaging phantom studies (e.g., Figure 5). However, **(B)** the number or mass concentration of AuNPs delivered to cells *in vitro* is initially increased with an increase in the initial mass concentration or dose of AuNPs delivered, but reaches a saturation point (gray shading), where a further increase in the initial dose of AuNPs does not lead to a greater mass concentration of AuNPs delivered or additional contrast enhancement.
AuNP: Gold nanoparticle; HU: Hounsfield unit; NP: Nanoparticle.

prising gold ions with atomic-scale dimensions, and a wide range of gold concentrations up to approximately 50 mM (~10 mg/ml; Figure 5). The x-ray attenuation of AuNPs and chloroauric acid solutions increased linearly with increasing gold concentration, as expected, but was independent of the particle diameter.

At the photon energy levels used in radiography and CT (10–140 keV), the x-ray attenuation of high atomic number elements is governed by photoelectric absorption due to differences in mass concentration, while scattering processes, which could be partially influenced by differences in specific surface area, are insignificant in comparison [19,43–44]. Thus, there should be no measurable effect of nanoparticle size on x-ray attenuation in x-ray absorption imaging systems. Any increase in x-ray attenuation with decreased AuNP diameter, such as that previously reported [36], is most likely to be due to colloidal instability. Colloidal instability of AuNP solutions comprising larger particle diameters results in a decreased mass concentration in solution and thus artificially low x-ray attenuation, due to the linear relationship discussed above (Figures 5 & 6A). Therefore, investigators should always carefully characterize the colloidal stability of AuNPs in media, as discussed further below, and verify gold concentrations using spectroscopic techniques [32].

The morphology of AuNPs was also shown to have no effect on x-ray attenuation at an equal mass concentration [84], as should be expected from the preceding discussion. However, various Au nanostructures and shapes (nanorods, nanoshells and nanocages, among others) have important utility in multifunctional applications, such as drug delivery and multimodal imaging [46,83,85]. For example, gold nanorods were used for simultaneous x-ray contrast and photothermal therapy, due to exhibiting a high absorption cross-section in the near-infrared region [46]. The design of multifunctional nanoparticle systems is an emerging area of research with significant current activity focused on theranostic nanoparticle agents [86].

Although the size and shape of AuNPs does not affect the x-ray attenuation for a given mass concentration, size and shape can significantly impact the delivery of a high mass concentration and thus contrast enhancement at the site of interest. For example, larger AuNPs (38 nm) that were targeted to lymph nodes *in vivo* enabled greater x-ray contrast compared with smaller targeted AuNPs (28 nm) [23]. The effects of AuNP size and shape on *in vivo* delivery and targeting are discussed in detail below.

Deliverability

The size of AuNPs affects colloidal stability, blood retention time and biodistribution, all of which govern the delivery of AuNPs *in vivo*. The colloidal stability of AuNPs is typically assessed by monitoring dispersion in solution by measuring the hydrodynamic diameter using dynamic light scattering, the location of the surface plasmon resonance peak using ultraviolet–visible spectroscopy and the ζ-potential (Figure 8). Each of these properties can also be measured over time and in response to changes in the *in vitro* environment (pH, temperature, medium and ionic strength) to investigate the potential for *in vivo* colloidal stability. Various media may include water, phosphate buffered saline and fetal bovine serum, among others. Colloidal stability is typically more difficult to achieve with increased AuNP size [32,87–88]. In classical Derjaguin–Landau–Verwey–Overbeek theory, colloidal stability is achieved when repulsive Coulomb forces (F_r) exceed attractive van der Waals forces (F_a) [89,90]. Attractive van der Waals forces are minimized with decreased particle diameter [87,89]. A systematic evaluation of AuNPs exhibiting various particle diameters with surface chemistry held constant demonstrated that 20 and 40 nm AuNPs were stable in physiologic media for over 48 h, while 80 nm AuNPs aggregated by 24 h [88].

Blood retention times must be sufficiently long to ensure passive or targeted delivery of AuNPs to the site of interest [34,35]. Long blood retention times may also be desirable for extending the available imaging window compared with iodinated agents [34,35]. The renal system exhibits a 6 nm cutoff diameter for glomerular

Table 1. The effects of gold nanoparticle size on passive targeting to cells *in vitro* and active targeting to mineral substrate *in vitro*.

Study (year)	AuNP size (nm)	Number of AuNPs/cell	ng AuNPs/cell†	AuNP description	Ref.
Passive targeting to HeLa cells					
Chithrani *et al.* (2006)	14	$3{\cdot}10^{3}$	$8.31{\cdot}10^{-8}$	Citrate-stabilized AuNPs	[51]
	30	$4.5{\cdot}10^{3}$	$1.23{\cdot}10^{-6}$		
	50	‡*$6{\cdot}10^{3}$*	$7.58{\cdot}10^{-6}$		
	74	$4{\cdot}10^{3}$	$1.64{\cdot}10^{-5}$		
	100	$2{\cdot}10^{3}$	*$2.02{\cdot}10^{-5}$*		
Xu *et al.* (2010)	4	*$1{\cdot}10^{7}$*	$6.46{\cdot}10^{-6}$	2-mercaptosuccinic acid-stabilized AuNPs	[36]
	20	$1{\cdot}10^{5}$	$8.08{\cdot}10^{-6}$		
	40	$2{\cdot}10^{4}$	$1.29{\cdot}10^{-5}$		
	60	$1{\cdot}10^{4}$	*$2.18{\cdot}10^{-5}$*		
Active targeting to mineral substrate		**Number of AuNPs/g mineral§**	**mg AuNPs/g mineral**		
Ross *et al.* (2014)	5	*$9.3{\cdot}10^{15}$*	11.0	Bisphosphonate-functionalized AuNPs	[32]
	13	$5.1{\cdot}10^{14}$	11.3		
	35	$7.0{\cdot}10^{13}$	29.3		
	76	$1.6{\cdot}10^{13}$	*62.5*		

†The mass of AuNPs delivered per cell was estimated from the reported number of AuNPs per cell, assuming perfectly spherical, monosized AuNPs and the bulk density of gold (19.3 g/cm^3).
‡Maximum values for the number and mass of delivered AuNPs are shown in italics. In each case, the largest AuNP size enabled delivery of the greatest mass concentration, but the smaller AuNP sizes enabled delivery of a greater number of AuNPs. Thus, since x-ray contrast is directly dependent on the mass concentration delivered and not the AuNP size, the metric for evaluating AuNPs as x-ray contrast agents should be the mass, and not the number of AuNPs delivered.
§The number of AuNPs delivered per mineral mass was estimated from the measured mass of AuNPs per mineral mass, assuming the mean particle dimensions and the bulk density of gold (19.3 g/cm^3).
AuNP: Gold nanoparticle.

filtration such that AuNPs less than this size are rapidly excreted through the kidney, typically within 5 min [18,91]. AuNPs larger than 10 nm have been detected in the blood 24 h after intravenous injection, indicating sufficient blood retention [92,93]. AuNPs with mean particle diameters of 15 and 50 nm exhibited greater retention in blood compared with 100 and 200 nm AuNPs after 24 h in mice [92]. However, another study reported that 100 nm AuNPs exhibited the greatest mass concentration in blood compared with 10, 50 or 250 nm AuNPs after 24 h in rats [93]. Differences in surface functionalization most likely account for these seemingly confounding results. The latter study investigated citrate coated AuNPs [93], while the former study suspended AuNPs in a sodium alginate solution to aid dispersion [92]. In both studies, AuNPs were already accumulated in other organs by 24 h. Therefore, differences in blood retention at this time point may not be critical for passive or targeted delivery. Thus, the blood retention time of AuNPs should be sufficient for adequate delivery as long as the diameter is greater than the glomerular filtration cutoff and the particles are stable *in vivo*.

The liver accumulates the highest concentration of AuNPs after intravenous delivery *in vivo*, regardless of the size of AuNPs [55]. Decreasing the size from approximately 250 to 10 nm increased the overall distribution of AuNPs to other organs, including the spleen, lungs, heart, kidneys and brain [88,92–93]. Moreover, AuNPs of up to 20 nm in diameter have been shown to cross the blood–brain barrier [92,94], which has been hypothesized to be due to a 20 nm gap formed between the astrocytic end-feet and capillary endothelium [95], but this has not been verified experimentally. However, no matter whether crossing the blood–brain barrier is viewed as a concern or desirable for targeted delivery

Table 2. Summary of doses and toxicity for *in vivo* investigations of gold nanoparticles as an x-ray contrast agent.

Study (year)	AuNP dose (mg/kg)	AuNP size (nm)	Surface	Model	Delivery method	Contrast enhancement	Toxicity	Ref.
Hainfeld *et al.* (2004)	2700, 1350	1.9	Citrate	Mouse	iv.	Tumor	None, ≤12 months	[17]
Hainfeld *et al.* (2006)	2700	1.9	Citrate	Mouse	iv.	Tumor and vasculature	None, ≤12 months	[18]
Cai *et al.* (2007)	492†	10	PEG	Mouse	iv.	Vasculature	None, ≤6 months‡	[34]
Guo *et al.* (2010)	492†	2–4	Acetylate dendrimer	Mouse	iv.	Vasculature	None, immediately after delivery	[37]
Peng *et al.* (2011)	394†	2–3	Acetylate dendrimer	Mouse	iv.	Vasculature	None, immediately after delivery	[42]
Peng *et al.* (2012)	393, 315†	2–4	PEG dendrimer	Mouse, rat	iv.	Vasculature	None	[57]
Kim *et al.* (2007)	133, 233†	30	PEG	Rat	iv.	Heart and liver tumor	None, ≤1 month	[35]
Alric *et al.* (2008)	120† 24, 72†	2.4	Gd chelate	Mouse Rat	iv.	Vasculature	None, ≤6 weeks	[58]
Boote *et al.* (2010)	86–99	20	Gum arabic	Pig	iv.	Liver and spleen	None§	[59]
Cole *et al.* (2014)	80	13	Bisphosphonate	Mouse	imam.	Microcalcifications	None	[60]
Peng *et al.* (2013)	79†	3.1	Folic acid, PEG dendrimer	Mouse	ip., iv.	Tumor	None¶	[61]

†Dose estimated from reported methods assuming 25 and 250 g body weights for mice and rats, respectively.
‡No evidence of inflammatory cell infiltration, cell swelling or tissue necrosis among the nine organs evaluated.
§No abnormalities detected during inspection of the dissected liver and spleen.
¶No morphological changes in the heart, lungs, liver, spleen, kidneys or intestines upon histological evaluation 1 month after delivery.
imam.: Intramammary; ip.: Intraperitoneal; iv.: Intravenous.

to brain tissue, a distinction must be made between AuNPs that actually penetrate the blood–brain barrier and accumulate in the brain tissue versus AuNPs that are retained in the cerebral intravascular network [94].

Only a few relevant studies have investigated the effects of AuNP morphology on delivery and biodistribution. Gold nanorods and nanoshells were shown to accumulate in the organs of the reticuloendothelial system after intravascular delivery [96], similar to AuNPs. Gold nanorods were shown to accumulate more rapidly in cells than AuNPs *in vitro* [51], which may be important for multimodal applications, such as drug delivery.

Targeting

AuNP size affects targeting or localization to the site of interest. A number of studies have investigated the influence of AuNP size on *in vitro* cellular internalization [36,51,97–98]. AuNPs can be internalized by cells through phagocytosis, micropinocytosis or receptor-mediated endocytosis [52]. The specific route for internalization is dependent on the surface chemistry, which will be discussed below, more than the AuNP size. However, receptor-mediated endocytosis of AuNPs was shown to be governed by the size of AuNPs. AuNPs with a 50 nm mean particle diameter were internalized at a faster rate compared with smaller (15 or 30 nm) and larger (74 or 100 nm) AuNPs, resulting in a greater number of AuNPs per cell [51]. However, it is also important to note that, for the targeted delivery of AuNPs as an x-ray contrast agent, the distinction between cellular internalization versus surface receptor binding may not be as critical compared with drug delivery applications.

The most important consideration of size in the targeted delivery of AuNPs as an x-ray contrast agent is to enable delivery of the greatest possible mass concentration of AuNPs to the site of interest, since x-ray attenuation is primarily dependent on mass concentration and not nanoparticle size. For example, the

mass of gold delivered to cells and the number AuNPs per cell can be calculated assuming perfectly spherical, monosized AuNPs and the bulk density of gold (19.3 g/cm^3). In two noteworthy studies investigating the effects of AuNP size on passive delivery [36,51], the maximum gold mass delivered per cell occurred at the largest particle size, while the maximum number of AuNPs delivered per cell occurred at a smaller particle size (Table 1). Therefore, the metric for the delivery of AuNPs as x-ray contrast agents should be the mass of gold delivered per cell, not the number of AuNPs per cell. This size effect has also been measured quantitatively for the active targeting of AuNPs to a noncellular inorganic substrate by comparing the binding affinity of differently sized AuNPs using Langmuir adsorption isotherms [32]. Larger AuNPs (76 nm) exhibited a greater binding affinity for the substrate compared with smaller AuNPs (5, 13 or 35 nm), resulting in a greater mass of AuNPs delivered per substrate mass despite a smaller number of AuNPs delivered per substrate mass (Table 1).

The localization of AuNPs within a tumor mass *in vivo* is highly dependent on AuNP size due to a 100–200 nm diameter of transvascular pores and fenestrations [91]. Therefore, AuNPs should be smaller than 100 nm for passive or active tumor targeting. Passively targeted AuNPs exhibited greater tumor uptake when 20 nm in size compared with either larger (40–80 nm) or smaller (4 nm) AuNPs [88]. However, another study reported that 20 nm AuNPs exhibited the lowest tumor accumulation compared with 40, 60, 80 and 100 nm AuNPs [99]. The discrepancy in these two studies is most likely due to differences in surface functionalization resulting in rapid blood clearance of the 20 nm AuNPs compared with the other sizes in the latter study [99], which will be discussed in the surface functionalization section.

Toxicity

AuNPs of less than 2 nm in size are more likely to induce toxicity than larger AuNPs (≥3 nm) [55–56,100–102], due to the ability of nanoparticles of less than 2 nm in size to irreversibly bind to biomolecules, including DNA [102]. AuNPs of greater than 3 nm in size are considered to be nontoxic *in vitro* and *in vivo* [55,56]; however, long-term toxicity is dependent on the accumulation of AuNPs in specific organs. Recall that 10–20 nm AuNPs exhibit the broadest biodistribution, resulting in more organs being exposed to AuNPs. On the other hand, larger AuNPs enable the delivery of a greater mass concentration but lower number of nanoparticles. Thus, systemic evaluations of the long-term toxicity of various sized AuNPs are needed at both the cellular and tissue level. Moreover, emphasis should be placed on evaluating potential liver toxicity, due to the liver exhibiting the greatest accumulation of AuNPs, regardless of size.

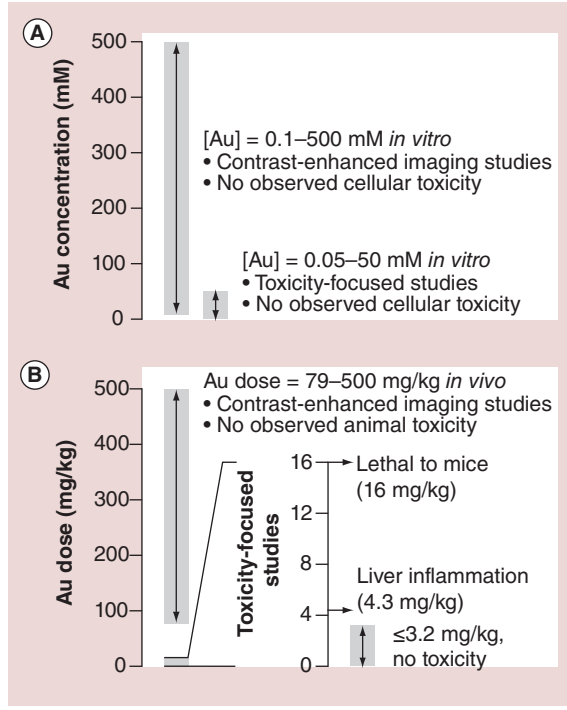

Figure 7. Summary of published data for the toxicity of gold nanoparticles. Studies are grouped by investigations on **(A)** cells *in vitro* and **(B)** animals *in vivo*, showing the range of Au concentrations and administered doses, respectively, examined by contrast-enhanced x-ray imaging studies versus toxicity-focused studies. There have been no observations of toxicity at the concentrations or doses of Au nanoparticles used for successful contrast-enhanced x-ray imaging, but these concentrations or doses are also typically greater than those investigated in toxicity-focused studies, suggesting a disconnect and the need for further study.

Gold linkages for surface functionalization

A significant advantage of AuNPs compared with other nanoparticles is their facile molecular surface functionalization [81] to promote colloidal stability and enable active targeting. Thiol [103–106], amine [103,107–109], disulfide [110,111], carboxylate [112] and phosphine [103,109,113–114] ligands, among others, have been used to form linkages with AuNP surfaces. Amine ligands are water soluble, form weak covalent bonds with gold and enable direct conjugation of amino acids for possible bioconjugation [107–109,115]. AuNPs of extremely small size (1–1.9 nm) can be synthesized with great control using phosphine ligands [113]. However, thiol ligands have been most widely used due to their strong covalent bonding with gold (30–40 kcal/mol) [116,117].

Giersig and Mulvaney introduced AuNP stabilization with alkanethiols, demonstrating that the

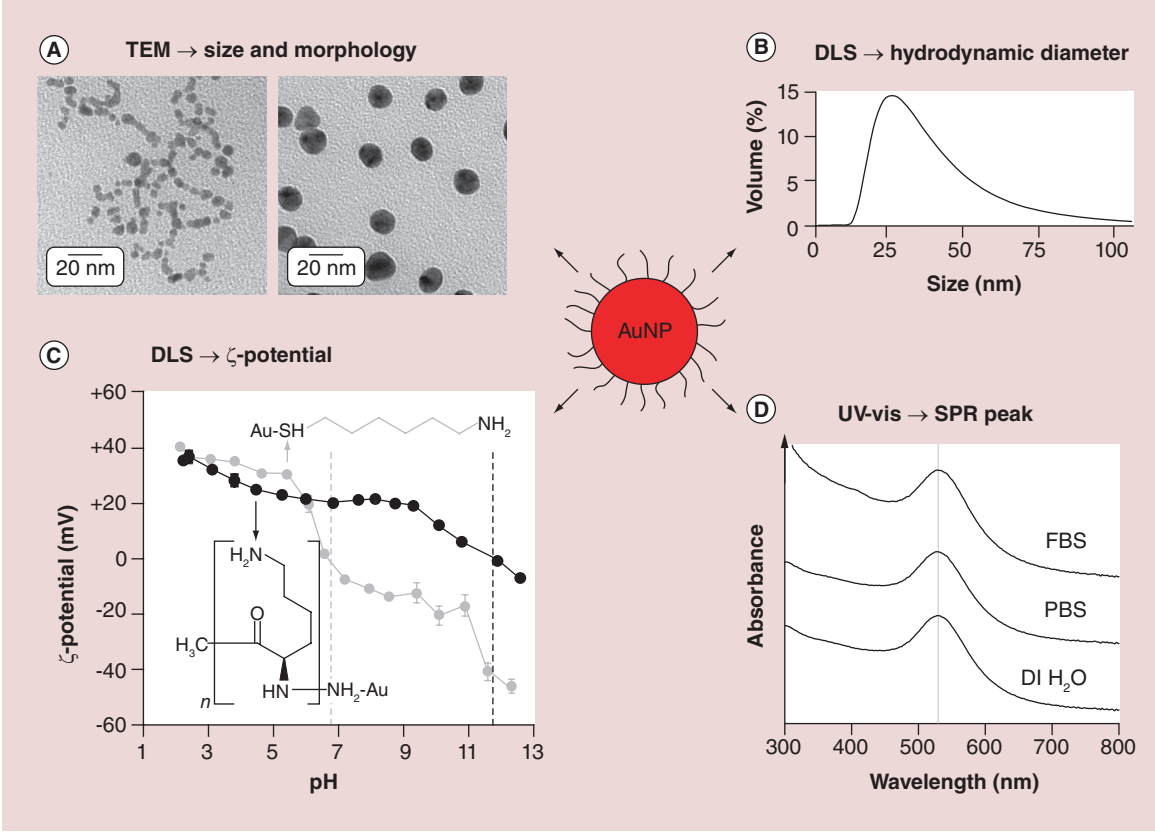

Figure 8. Common methods for characterizing the size and colloidal stability of gold nanoparticles. (A) TEM is used to measure the physical particle size, morphology and size/morphology distributions. **(B)** DLS is used to measure the hydrodynamic particle diameter. **(C)** The surface charge or ζ-potential is measured using DLS and other techniques. For example, AuNPs surface functionalized with poly-L-lysine (black) and 6-amino-1-hexanethiol (gray) exhibit significant differences in the isoelectric point (dashed lines). Error bars show one standard deviation of the mean and error bars that are not shown lie within the data point. **(D)** UV-vis is used to measure the SPR peak, which is indicative of size, shape and aggregation. Note that DLS and UV-vis are particularly useful for investigating the effects of time, pH, medium and surface functionalization, as shown.
AuNP: Gold nanoparticle; DI H_2O: Distilled water; DLS: Dynamic light scattering; FBS: Fetal bovine serum; PBS: Phosphate-buffered saline; SPR: Surface plasmon resonance; TEM: Transmission electron microscopy; UV-vis: Ultraviolet–visible spectroscopy.

spacing between monolayers of AuNPs was dependent on the length of the alkanethiol [104]. Subsequently, the Brust method for single-phase synthesis of thiol-stabilized AuNPs significantly impacted the field due to the ease of synthesizing thermally stable and air-stable AuNPs that could be dried and redispersed in a range of solvents [105,106]. The thiol–gold bond strength and molecular structure is well characterized on bulk gold surfaces with the formation of self-assembled monolayers [116]; however, the chemical stability of ligands on the highly curved surfaces of AuNPs likely differs from the bulk properties. For amine–gold linkages, a finite number of amine ligands were able to be adsorbed onto the surface of AuNPs, and the ligand density decreased with increased AuNP diameter [107].

Dendrimers provide another approach for linking molecules to AuNPs. Poly(amidoamine) dendrimers have been most commonly used and act as templates for forming dendrimer-entrapped AuNPs systems [118–120]. Dendrimer-entrapped AuNPs can be further surface functionalized through the modification of the dendrimer molecules for improved cytocompatibility [42,121], colloidal stability [57] and active targeting [61,71,122–123]. The advantages of dendrimer-entrapped AuNPs include colloidal stability over a wide range of environmental conditions (pH, ionic strength and temperature) due to the protective dendrimer arms, and the ability to conjugate known quantities of biomolecules on the terminal arms of the dendrimers [81]. Dendrimer-entrapped AuNPs may have greater potential for cytotoxicity due to the positively charged amine-terminated arms of poly(amidoamine) dendrimers, although acetylation has been used to neutralize the charge and reduce toxicity [121]. The AuNP size in dendrimer-entrapped systems used as x-ray

contrast agents has been quite small (≤8 nm) [37–38,40,42,57,61,71,121–125], with no indication of whether or not larger AuNPs could be used to deliver a greater mass concentration and no measurements of the hydrodynamic particle diameter. Finally, note that the use of dendrimer-entrapped AuNPs as x-ray contrast agents was not distinguished from other AuNP systems elsewhere in this article, since the design of these soft nanoparticles [126] involves the same key structural characteristics (Figure 3).

Surface functionalization

Many different types of molecules can be attached to the surface of AuNPs, using the linkages described above, in order to improve colloidal stability and enable active targeting. Surface functionalization of AuNPs with PEG has been the most widely studied. The addition of PEG onto AuNP surfaces improves colloidal stability by reducing the nonspecific adsorption of serum proteins and preventing agglomeration through steric interactions of the PEG brushes [127]. Other molecules that have been investigated for improving colloidal stability include gum arabic [59,128], polyacrylic acid [63], polysaccharides [20,48] and polyvinyl alcohol [32,73,84,129–131]. AuNPs have been surface functionalized with peptides [21,72], antibodies [23,47,63–64,69–70], saccharides [20,48,66–67], lipoproteins [22,132] and numerous small molecules [32,61,71,73,122–123,125,129–131] for active targeting. Molecular ligands can be strategically chosen for target-specific binding to a site of interest, including cancerous cells or tumors [21,33,47–48,61,63–72,122–125], the liver [20], lymph nodes [23], atherosclerotic plaque [22] and bone or mineral deposits [32,60,73,129–131]. Active targeting to a site of interest enables specific contrast enhancement (Figure 9). AuNP surfaces can also be functionalized with combinations of molecules designed for promoting both colloidal stability and active targeting capabilities [20,23,47,61,64,69,133].

Deliverability

Surface functionalization affects the deliverability of AuNPs through improved colloidal stability, longer blood retention and a wider biodistribution compared with bare AuNPs. The stability of citrate-stabilized AuNPs is dominated by repulsive electrostatic forces between the equally charged citrate molecules present near the surface [89]. However, these repulsive forces can be shielded due to the ionic strength of the physiological media, resulting in agglomeration due to attractive van der Waals forces [53,55,89]. In addition, changes in pH can alter the surface charge of AuNPs and lead to agglomeration [90,134]. Therefore, additional surface modification is necessary in order to stabilize AuNPs through means other than electrostatic interactions. PEG improves stability through steric effects [135], as evidenced by a shift in ζ-potential to a more neutral charge compared with the highly negative charge of citrate-stabilized AuNPs [88,136]. The steric stabilization of PEGylated AuNPs enables *in vitro* colloidal stability in solutions of high ionic strength and over a wide range of pH and temperature [57,61,88,125,133].

PEGylation increases the blood half-life of AuNPs *in vivo* [91]. When injected into the bloodstream, bare AuNPs are quickly marked by opsonin proteins for phagocytosis by macrophages [137]. Rapid blood clearance dramatically reduces the utility of AuNPs as an x-ray contrast agent by limiting the mass concentration that is able to reach the site of interest. Therefore, preventing opsonization of AuNPs is critical, and one strategy is to coat the surface with a polymer, such as PEG, which blocks electrostatic or hydrophobic interactions with serum proteins [137]. A longer half-life can be achieved with increased PEG chain length. For example, 18 nm AuNPs coated with 2 kDa PEG molecules exhibited a half-life of approximately 4 h compared with approximately 51 h with 10 kDa PEG molecules [91,99]. For reference, a clinically available iodine-based contrast agent, Ultravist® (Bayer Healthcare, NJ, USA), exhibits a blood half-life of <10 min [35,49].

An increased retention time is advantageous not only for blood pool imaging, but also for passive and active targeting. For blood pool imaging applications, enhanced vascular retention increases the available imaging window, which is a known limitation of iodine-based contrast agents [49]. Both passive and active targeting rely on the accumulation of AuNPs within the site of interest, whether nonspecific or specific, respectively. Accumulation is dependent on sufficient circulation of AuNPs in the bloodstream [91], as well the kinetics of the dynamic exchange of AuNPs being taken up by cells/tissues and cleared back into the bloodstream [138]. The longer that AuNPs can circulate without being removed from the bloodstream by macrophages, the greater the likelihood of accumulation at the site of interest.

The overall biodistribution of surface-functionalized AuNPs is also dependent on improved colloidal stability and increased vascular retention. Surface-functionalized AuNPs are more widely distributed compared with bare AuNPs due to a longer blood half-life [91], although the effects of AuNP size must also be considered, as discussed above. The surface functionalization of AuNPs was initially intended to decrease the accumulation of AuNPs in the liver and increase accumulation within the site of interest through passive or active targeting. However, the largest accumulation of surface-functionalized AuNPs is still in the liver or

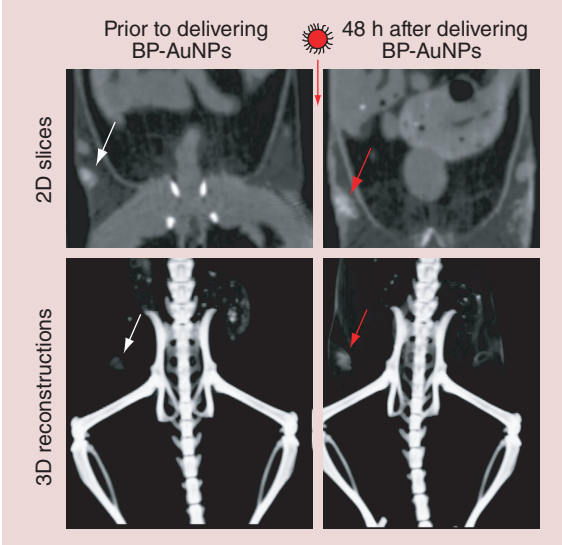

Figure 9. 2D slices and 3D computed tomography reconstructions showing microcalcifications in murine mammary glands (white arrows) before and 48 h after intramammary delivery of bisphosphonate-functionalized gold nanoparticles *in vivo*. BP-AuNPs enabled contrast-enhanced detection of microcalcifications (red arrows) due to specific binding interactions, retention in the microcalcification site and clearance from the contralateral control site [60]. BP-AuNP: Bisphosphonate-functionalized gold nanoparticle.

spleen, although surface functionalization appears to increase the time required for AuNPs to accumulate in these organs [21,55].

Targeting

Surface functionalization is a powerful tool to enable passive or active targeting of AuNPs to a site of interest. The most commonly investigated site of interest has been tumors. Passive targeting relies on the 'leaky' vasculature of tumors and the enhanced permeability and retention effect for the accumulation of AuNPs in a tumor [26]. AuNPs can escape vessels and enter the tumor through transvascular pores formed by a distortion of the endothelial layer of blood vessels feeding the tumor. Surface-functionalized AuNPs increase the blood circulation time, which increases the probability of AuNPs accumulating within a tumor [91]. Passive targeting of surface-functionalized AuNPs to tumor xenografts resulted in an approximately two-fold increase in the x-ray attenuation of the tumor compared with before the delivery of AuNPs [35,57,69,136].

Many *in vitro* studies have shown that actively targeted AuNPs are internalized by cells that are positive for the receptor in greater amounts compared with nontargeted AuNPs [61,63,66–67,69,71–72,125] or when incubated with cells that lack the receptor [47–48,61,64,68,125]. Actively targeted AuNPs have also exhibited site-specific accumulation and enabled contrast-enhanced radiographic imaging *in vivo* (Table 3). For example, EGFR-targeted AuNPs enabled a 5.6-fold greater contrast enhancement compared with nontargeted AuNPs in tumors [69]. Heparin-functionalized AuNPs enabled 12.6- and 3.2-fold increases in the x-ray attenuation of the liver compared with saline or iodine, respectively, due to the specificity of heparin for Kupffer cells [20]. Thus, targeted AuNP x-ray contrast agents provide a means to utilize CT for molecular imaging. Molecular imaging is the visualization of molecular processes through the use of biomarkers. Current molecular imaging techniques utilize PET, SPECT, optical imaging (e.g., fluorescence and bioluminescence, among others) and MRI. However, the surface functionalization of AuNPs for active targeting could enable a transformational shift in CT from an anatomic imaging modality to a combined anatomic and molecular imaging modality.

Toxicity

The effect of surface functionalization on toxicity is related to the altered biodistribution of surface-functionalized AuNPs compared with bare AuNPs. However, as mentioned previously, the majority of AuNPs administered *in vivo* accumulate in the liver. A goal of active targeting is to reduce the accumulation of AuNPs in nontargeted organs. Unfortunately, this goal has not been realized for the intravascular delivery of targeted AuNPs. For example, targeted AuNPs exhibited improved tumor accumulation compared with nontargeted AuNPs, but the accumulated mass of AuNPs delivered to the site of interest was still an order of magnitude lower than that in the liver or spleen [91]. Localized delivery (e.g., intratumoral and intramammary) has notably improved the accumulation in the site interest relative to other organs [60,71–72,139] and may offer an alternative means for delivering the necessary mass concentration to the site of interest while reducing liver accumulation.

Conclusion & future perspective

Over the last decade, there has been significant progress in the design of AuNP x-ray contrast agents to meet the necessary functional requirements (Figures 2 & 3) for blood pool imaging, passive targeting and active targeting applications (Figure 1). However, there is still much work to be done if AuNP x-ray contrast agents are to be clinically translated. Current x-ray imaging techniques provide high spatial and temporal resolution, but lower sensitivity compared with PET and MRI, and no ability for molecular imaging. Therefore, efforts to improve sensitivity should continue to focus not only on improvements in instrumentation (e.g., dual-energy CT and spectral CT) and reconstruction algorithms, but also new and optimized x-ray contrast agents. Stud-

Table 3. Chronological summary of investigations reporting contrast enhancement (ΔHU) by actively targeted gold nanoparticles *in vivo*.

Study (year)	AuNP size (nm)	Surface functionalization	AuNP dose (mg/kg)	Delivery route	Target	ΔHU†	Time point (h)	Ref.
Sun *et al.* (2009)	20	Heparin	250	iv.	Liver	447 vs PEG control	2	[20]
Chanda *et al.* (2010)	16–18	Bombesin	12‡	ip.	Prostate tumor cells	150 vs predelivery	1	[21]
Cormode *et al.* (2010)	3.1	High-density lipid	500	iv.	Atherosclerotic plaque	Detectable vs iodine and calcium phosphate	24	[22]
Eck *et al.* (2010)	28 38	Anti-CD4-PEG	56‡	iv.	Lymph nodes	35 vs PEG control 55 vs PEG control	1 48	[23]
Hainfeld *et al.* (2011)	15	Anti-HER-PEG	1100	iv.	$HER2^+$ tumor	8.3 vs 6.2% ID for $HER2^-$ tumor control	20	[47]
Reuveni *et al.* (2011)	30	Anti-EGFR-PEG	200‡	iv.	Skin tumor	112 vs PEG control	6	[69]
Peng *et al.* (2013)	3.1	FA–PEG–DEN	79‡	it., ip.	HeLa cell tumor	20 vs PEG–DEN control	6	[61]
Wang *et al.* (2013)	3.1	FA–DEN	79‡	ip. iv. it.	Lung cancer cells	20 vs predelivery 25 vs predelivery 150 vs predelivery	6	[71]
Liu *et al.* (2013)	6.5	FA–DEN	92‡	iv.	HeLa cell tumor	10 vs DEN control	1	[123]
Chen *et al.* (2013)	4.0	FA–PEG–Gd–DEN	158‡	iv.	HeLa cell tumor	60 vs PEG–Gd–DEN control	24	[125]
Sun *et al.* (2014)	20	Glycol chitosan	200‡	it.	Colon cancer cells	$\Delta\mu = 1.222\ cm^{-1}$ vs heparin	2	[48]
Shilo *et al.* (2014)	20	Insulin–PEG	240	iv.	Insulin receptors in the brain	5 vs 0.5% ID for PEG control	2	[94]
Cole *et al.* (2014)	13	Bisphosphonate	80	imam.	Microcalcifications	135 vs no microcal 65 vs predelivery	48	[60]

†The maximum ΔHU for each study is reported, but most reported contrast for more than one control group and multiple time points.
‡Dose estimated from reported methods assuming 25- and 250-g body weights for mice and rats, respectively.
AuNP: Gold nanoparticle; DEN: Dendrimer; EGFR: EGF receptor; HU: Hounsfield unit; FA: Folic acid; Gd: Gadolinium; ID: Injected dose; imam.: Intramammary; ip.: Intraperitoneal; it.: Intratumoral; iv.: Intravenous; μ: linear x-ray attenuation coefficient (cm^{-1}).

ies comparing different x-ray contrast agents must take care to consider the effects of the x-ray source energy spectra relative to contrast agent absorption edges (Figure 4) and potential differences in mass concentration due to differences in colloidal stability and delivery. Considering these effects, AuNPs are a promising x-ray contrast agent for CT and mammography.

The most critical factor governing contrast enhancement is the mass concentration of AuNPs delivered and retained at the site of interest. Therefore, future research should focus on improving the *in vivo* delivery and targeting of AuNPs to the site of interest. Simply increasing the administered dose does not guarantee accumulation of a higher mass concentration of AuNPs at the site of interest [74]. Once active receptors or the targeted substrate become saturated, the increase in mass concentration delivered with increased initial dose diminishes (Figure 6) [32,36,51]. However, this effect is not well understood, especially for the targeted delivery of AuNPs, and should be a focus for fundamental research. An increased dose is also more likely to cause adverse side effects, including toxicity [55]. There appears to be a growing consensus regarding the low cytotoxicity of AuNPs *in vitro*, but there has been limited rigorous evaluation of the *in vivo* cytotoxicity of AuNP x-ray contrast agents (Figure 7 & Table 2), particularly for the liver and spleen, which typically accumulate the highest concentrations of AuNPs after delivery

[55]. Therefore, dosing studies are critical for determining the minimum dose required to enhance contrast without inducing cytotoxicity in a given application and model.

The size and surface chemistry of functionalized AuNPs do not have a direct effect on contrast enhancement (Figure 5), but are critical for delivery, targeting and toxicity. The AuNP size should be greater than approximately 3 nm for nontoxicity [100–102], greater than approximately 6 nm to avoid renal filtration [18,91] and achieve a sufficient blood retention, and less than the diameter of transvascular pores (~100 nm) for passive or active tumor targeting [91]. Decreased AuNP size generally results in a broader biodistribution to nontargeted organs and tissues [88,92–93], while increased size enables the delivery of a greater mass concentration but lower number of AuNPs per targeted cell or substrate (Table 1). Evaluations of AuNPs as x-ray contrast agents should use the mass concentration, and not the number of AuNPs delivered per targeted cell or substrate as the figure of merit. Thus, the AuNP size for x-ray contrast agents should be as large as possible in order to maximize the delivered mass concentration, but not too large so as to compromise colloidal stability, blood retention, cellular uptake or targeting.

The facile surface functionalization of AuNPs provides a seemingly unlimited toolbox for manipulating colloidal stability and targeted delivery. PEGylated AuNPs have been most commonly utilized for achieving robust colloidal stability in physiological media through steric stabilization and extending the blood retention time for imaging and delivery [91,127,135]. Various molecular ligands have enabled targeted delivery and contrast enhancement at sites of interest, including cancerous cells or tumors, organs and mineral deposits (Table 3). On the other hand, surface functionalization strategies have not yet solved the challenge of decreasing the nontargeted accumulation in organs such as the liver and spleen while increasing accumulation within the targeted site of interest. Surface-functionalized AuNPs have the potential to be the enabling technology for molecular imaging with CT (Figure 9), but concerted

Executive summary

Background

- Computed tomography enables 3D anatomic imaging at high spatial resolution, but requires delivery of an x-ray contrast agent in order to distinguish tissues with similar or low x-ray attenuation.
- Gold nanoparticles (AuNPs) have gained recent attention as an x-ray contrast agent due to exhibiting high x-ray attenuation, nontoxicity and facile synthesis and surface functionalization for colloidal stability and targeted delivery.
- Design of AuNPs is achieved by strategically controlling key structural characteristics (composition, mass concentration, size, shape and surface functionalization) for optimized properties and functional performance.

Composition

- The composition of an x-ray contrast agent governs x-ray attenuation at a given photon energy level and therefore the ability to provide contrast enhancement.
- Materials or tissues with high atomic numbers and bulk densities, such as gold, generally absorb more x-rays.
- AuNPs have provided significantly greater x-ray attenuation compared with iodine at low (40–60 kVp) tube potentials and especially above the gold *K*-edge at the high (100–140 kVp) tube potentials that are relevant to clinical computed tomography.

Mass concentration

- X-ray attenuation increases with mass concentration; therefore, delivery of a larger mass concentration of AuNPs to the site of interest will increase contrast enhancement.

Size & morphology

- The size and shape of AuNPs does not directly affect x-ray attenuation, but does influence the delivery of a high mass concentration and thus contrast enhancement at the site of interest.
- The AuNP size for x-ray contrast agents should be as large as possible in order to maximize the delivered mass concentration, but not too large so as to compromise colloidal stability, blood retention, cellular uptake or targeting.

Surface functionalization

- Facile synthesis and molecular surface functionalization to promote colloidal stability and enable active targeting is a significant advantage of AuNPs compared with other nanoparticles.
- A nearly limitless variety of molecules can be attached to the surface of AuNPs, commonly using thiol, amine, disulfide, carboxylate and phosphine ligands to form linkages with AuNP surfaces.
- The most widely studied modification has been the surface functionalization of AuNPs with PEG for colloidal stability.

research and development efforts will be required in order to meet this goal.

Financial & competing interests disclosure

Funding sources: National Science Foundation (DMR-1309587), Walther Cancer Foundation; St Joseph Regional Medical Center; Indiana Clinical and Translational Sciences Institute (NIH grant RR025761); and US Army Medical Research and Material Command (W81XWH-06-1-0196) through the Peer Reviewed Medical Research Program (PR054672). The authors have no other relevant affiliations or financial involvement with any organization or entity with a financial interest in or financial conflict with the subject matter or materials discussed in the manuscript apart from those disclosed.

No writing assistance was utilized in the production of this manuscript.

References

Papers of special note have been highlighted as:
• of interest; •• of considerable interest

1 Yu S-B, Watson AD. Metal-based x-ray contrast media. *Chem. Rev.* 99(9), 2353–2377 (1999).

2 Goldman LW. Principles of CT and CT technology. *J. Nucl. Med. Technol.* 35(3), 115–128 (2007).

3 de GonzÃ¡lez AB, Mahesh M, Kim K-P *et al.* Projected cancer risks from computed tomographic scans performed in the United States in 2007. *Arch. Intern. Med.* 169(22), 2071–2077 (2009).

4 Kalender WA. X-ray computed tomography. *Phys. Med. Biol.* 51(13), R29–R43 (2006).

5 Wang G, Yu H, De Man B. An outlook on x-ray CT research and development. *Med. Phys.* 35(3), 1051–1064 (2008).

6 Flohr TG, McCollough CH, Bruder H *et al.* First performance evaluation of a dual-source CT (DSCT) system. *Eur. Radiol.* 16(2), 256–268 (2006).

7 Roessl E, Proksa R. K-edge imaging in x-ray computed tomography using multi-bin photon counting detectors. *Phys. Med. Biol.* 52(15), 4679–4696 (2007).

8 Anderson NG, Butler AP. Clinical applications of spectral molecular imaging: potential and challenges. *Contrast Media Mol. Imaging* 9(1), 3–12 (2014).

9 Elliott A. Medical imaging. *Nucl. Instrum. Meth. A* 546(1–2), 1–13 (2005).

10 Kircher MF, Willmann JK. Molecular body imaging: MR imaging, CT, and US. Part I. Principles. *Radiology* 263(3), 633–643 (2012).

11 Goldman LW. Principles of CT: radiation dose and image quality. *J. Nucl. Med. Technol.* 35(4), 213–225 (2007).

12 Lee N, Choi SH, Hyeon T. Nano-sized CT contrast agents. *Adv. Mater.* 25(19), 2641–2660 (2013).

13 Osborne ED, Sutherland CG, School AJ, Rowntree LG. Roentgenography of urinary tract during excretion of sodium iodide. *JAMA* 250(20), 2848–2853 (1923).

14 Lusic H, Grinstaff MW. X-ray–computed tomography contrast agents. *Chem. Rev.* 113(3), 1641–1666 (2013).

• **Recent and thorough review of all types of x-ray contrast agents, including gold nanoparticles (AuNPs).**

15 Hallouard F, Anton N, Choquet P, Constantinesco A, Vandamme T. Iodinated blood pool contrast media for preclinical x-ray imaging applications – a review. *Biomaterials* 31(24), 6249–6268 (2010).

16 Rhee CM, Bhan I, Alexander EK, Brunelli SM. Association between iodinated contrast media exposure and incident hyperthyroidism and hypothyroidism. *Arch. Intern. Med.* 172(2), 153–159 (2012).

17 Hainfeld JF, Slatkin DN, Smilowitz HM. The use of gold nanoparticles to enhance radiotherapy in mice. *Phys. Med. Biol.* 49(18), N309–N315 (2004).

18 Hainfeld JF, Slatkin DN, Focella TM, Smilowitz HM. Gold nanoparticles: a new x-ray contrast agent. *Br. J. Radiol.* 79(939), 248–253 (2006).

•• **First study to demonstrate the potential of AuNPs as an x-ray contrast agent.**

19 Hubbell JH, Seltzer SM. Tables of x-ray mass attenuation coefficients and mass energy–absorption coefficients (version 1.4). National Institute of Standards and Technology, MD, USA (2004). www.nist.gov/pml/data/xraycoef/index.cfm

20 Sun I-C, Eun D-K, Na JH *et al.* Heparin-coated gold nanoparticles for liver-specific CT imaging. *Chem. Eur. J.* 15(48), 13341–13347 (2009).

21 Chanda N, Kattumuri V, Shukla R *et al.* Bombesin functionalized gold nanoparticles show *in vitro* and *in vivo* cancer receptor specificity. *Proc. Natl Acad. Sci. USA* 107(19), 8760–8765 (2010).

22 Cormode DP, Roessl E, Thran A *et al.* Atherosclerotic plaque composition: analysis with multicolor CT and targeted gold nanoparticles. *Radiology* 256(3), 774–782 (2010).

23 Eck W, Nicholson AI, Zentgraf H, Semmler W, Bartling S. Anti-CD4-targeted gold nanoparticles induce specific contrast enhancement of peripheral lymph nodes in x-ray computed tomography of live mice. *Nano Lett.* 10(7), 2318–2322 (2010).

24 Shilo M, Reuveni T, Motiei M, Popovtzer R. Nanoparticles as computed tomography contrast agents. *Nanomedicine* 7(2), 257–269 (2012).

25 Jakhmola A, Anton N, Vandamme TF. Inorganic nanoparticles based contrast agents for x-ray computed tomography. *Adv. Healthc. Mater.* 1(4), 413–431 (2012).

26 Brannon-Peppas L, Blanchette JO. Nanoparticle and targeted systems for cancer therapy. *Adv. Drug Deliv. Rev.* 56(11), 1649–1659 (2004).

27 Brigger I, Dubernet C, Couvreur P. Nanoparticles in cancer therapy and diagnosis. *Adv. Drug Deliv. Rev.* 54(5), 631–651 (2002).

28 Tomalia DA. In quest of a systematic framework for unifying and defining nanoscience. *J. Nanopart. Res.* 11(6), 1251–1310 (2009).

29 Kannan RM, Nance E, Kannan S, Tomalia DA. Emerging concepts in dendrimer-based nanomedicine: from design

principles to clinical applications. *J. Intern. Med.* 276(6), 579–617 (2014).

30 Säbel M, Aichinger H. Recent developments in breast imaging. *Phys. Med. Biol.* 41(3), 315–368 (1996).

31 Huda W, Gkanatsios NA. Radiation dosimetry for extremity radiographs. *Health Phys.* 75(5), 492–499 (1998).

32 Ross RD, Cole LE, Tilley JMR, Roeder RK. Effects of functionalized gold nanoparticle size on x-ray attenuation and substrate binding affinity. *Chem. Mater.* 26(2), 1187–1194 (2014).

• **Recent study demonstrating that x-ray attenuation is not dependent on AuNP size.**

33 Rigley S, Rigon L, Ataelmannan K *et al.* Absorption edge subtraction imaging for volumetric measurement in an animal model of malignant brain tumor. *Nucl. Instrum. Meth. A* 548(1–2), 88–93 (2005).

34 Cai Q-Y, Kim SH, Choi KS *et al.* Colloidal gold nanoparticles as a blood-pool contrast agent for x-ray computed tomography in mice. *Invest. Radiol.* 42(12), 797–806 (2007).

35 Kim D, Park S, Lee JH, Jeong YY, Jon S. Antibiofouling polymer-coated gold nanoparticles as a contrast agent for *in vivo* x-ray computed tomography imaging. *J. Am. Chem. Soc.* 129(24), 7661–7665 (2007).

36 Xu C, Tung GA, Sun S. Size and concentration effect of gold nanoparticles on x-ray attenuation as measured on computed tomography. *Chem. Mater.* 20(13), 4167–4169 (2008).

37 Guo R, Wang H, Peng C *et al.* X-ray attenuation property of dendrimer-entrapped gold nanoparticles. *J. Phys. Chem. C* 114(1), 50–56 (2010).

38 Kojima C, Umeda Y, Ogawa M, Harada A, Magata Y, Kono K. X-ray computed tomography contrast agents prepared by seeded growth of gold nanoparticles in PEGylated dendrimer. *Nanotechnology* 21(24), 245104 (2010).

39 Jackson PA, Rahman WNWA, Wong CJ, Ackerly T, Geso M. Potential dependent superiority of gold nanoparticles in comparison to iodinated contrast agents. *Eur. J. Radiol.* 75(1), 104–109 (2010).

40 Wang H, Zheng L, Guo R *et al.* Dendrimer-entrapped gold nanoparticles as potential CT contrast agents for blood pool imaging. *Nanoscale Res. Lett.* 7, 190 (2012).

41 Galper MW, Saung MT, Fuster V *et al.* Effect of computed tomography scanning parameters on gold nanoparticle and iodine contrast. *Invest. Radiol.* 47(8), 475–481 (2012).

42 Peng C, Wang H, Guo R *et al.* Acetylation of dendrimer-entrapped gold nanoparticles: synthesis, stability, and x-ray attenuation properties. *J. Appl. Polym. Sci.* 119(3), 1673–1682 (2011).

43 Berger MJ, Hubbell JH, Seltzer SM *et al.* XCOM: photon cross section database (version 1.5). National Institute of Standards and Technology, MD, USA (2010). www.nist.gov/pml/data/xcom/index.cfm

44 Hubbell JH, Gimm HA, Overbo IJ. Pair, triplet, and total atomic cross sections (and mass attenuation coefficients) for 1 MeV–100 GeV photons in elements Z=1 to 100. *J. Phys. Chem. Ref. Data* 9, 1023–1147 (1980).

45 Willmann JK, van Bruggen N, Dinkelborg LM, Gambhir SS. Molecular imaging in drug development. *Nat. Rev. Drug Discov.* 7(7), 591–607 (2008).

46 Huang P, Le Bao, Zhang C *et al.* Folic acid-conjugated silica-modified gold nanorods for x-ray/CT imaging-guided dual-mode radiation and photo-thermal therapy. *Biomaterials* 32(36), 9796–9809 (2011).

47 Hainfeld JF, O'Connor MJ, Dilmanian FA, Slatkin DN, Adams DJ, Smilowitz HM. Micro-CT enables microlocalisation and quantification of Her2-targeted gold nanoparticles within tumour regions. *Br. J. Radiol.* 84(1002), 526–533 (2011).

48 Sun I-C, Na JH, Jeong SY *et al.* Biocompatible glycol chitosan-coated gold nanoparticles for tumor-targeting CT imaging. *Pharm. Res.* 31(6), 1418–1425 (2014).

49 Krause W. Delivery of diagnostic agents in computed tomography. *Adv. Drug Deliv. Rev.* 37(1–3), 159–173 (1999).

50 Kouris K, Spyrou NM, Jackson DF. Minimum detectable quantities of elements and compounds in a biological matrix. *Nucl. Instrum. Meth. Phys. Res.* 187(2–3), 539–545 (1981).

51 Chithrani BD, Ghazani AA, Chan WCW. Determining the size and shape dependence of gold nanoparticle uptake into mammalian cells. *Nano Lett.* 6(4), 662–668 (2006).

52 Conner SD, Schmid SL. Regulated portals of entry into the cell. *Nature* 422, 37–44 (2003).

53 Albanese A, Chan WCW. Effect of gold nanoparticle aggregation on cell uptake and toxicity. *ACS Nano* 5(7), 5478–5489 (2011).

54 Mahmoudi M, Lynch I, Ejtehadi MR, Monopoli MP, Bombelli FB, Laurent S. Protein–nanoparticle interactions: opportunities and challenges. *Chem. Rev.* 111(9), 5610–5637 (2011).

55 Khlebtsov N, Dykman L. Biodistribution and toxicity of engineered gold nanoparticles: a review of *in vitro* and *in vivo* studies. *Chem. Soc. Rev.* 40(3), 1647–1671 (2011).

•• **Comprehensive and insightful review of the current state of knowledge regarding the biodistribution and toxicity of AuNPs.**

56 Alkilany AM, Murphy CJ. Toxicity and cellular uptake of gold nanoparticles: what we have learned so far? *J. Nanopart. Res.* 12(7), 2313–2333 (2010).

57 Peng C, Zheng L, Chen Q *et al.* PEGylated dendrimer-entrapped gold nanoparticles for *in vivo* blood pool and tumor imaging by computed tomography. *Biomaterials* 33(4), 1107–1119 (2012).

58 Alric C, Taleb J, Le Duc G *et al.* Gadolinium chelate coated gold nanoparticles as contrast agents for both x-ray computed tomography and magnetic resonance imaging. *J. Am. Chem. Soc.* 130(18), 5908–5915 (2008).

59 Boote E, Fent G, Kattumuri V *et al.* Gold nanoparticle contrast in a phantom and juvenile swine: models for molecular imaging of human organs using x-ray computed tomography. *Acad. Radiol.* 17(4), 410–417 (2010).

60 Cole LE, Vargo-Gogola T, Roeder RK. Contrast-enhanced x-ray detection of breast microcalcifications in a murine

model using targeted gold nanoparticles. *ACS Nano* 8(7), 7486–7496 (2014).

61 Peng C, Qin J, Zhou B *et al.* Targeted tumor CT imaging using folic acid-modified PEGylated dendrimer-entrapped gold nanoparticles. *Polym. Chem.* 4(16), 4412–4424 (2013).

62 Sinha R, Kim GJ, Nie S, Shin DM. Nanotechnology in cancer therapeutics: bioconjugated nanoparticles for drug delivery. *Mol. Cancer Ther.* 5(8), 1909–1917 (2006).

63 Popovtzer R, Agrawal A, Kotov NA *et al.* Targeted gold nanoparticles enable molecular CT imaging of cancer. *Nano Lett.* 8(12), 4593–4596 (2008).

• **First study demonstrating the use of targeted AuNPs for x-ray imaging.**

64 Eck W, Craig G, Sigdel A *et al.* PEGylated gold nanoparticles conjugated to monoclonal F19 antibodies as targeted labeling agents for human pancreatic carcinoma tissue. *ACS Nano* 2(11), 2263–2272 (2008).

65 Chanda N, Shukla R, Katti KV, Kannan R. Gastrin releasing protein receptor specific gold nanorods: breast and prostate tumor avid nanovectors for molecular imaging. *Nano Lett.* 9(5), 1798–1805 (2009).

66 Aydogan B, Li J, Rajh T *et al.* AuNP-DG: deoxyglucose-labeled gold nanoparticles as x-ray computed tomography contrast agents for cancer imaging. *Mol. Imaging Biol.* 12(5), 463–467 (2010).

67 Li J, Chaudhary A, Chmura SJ *et al.* A novel functional CT contrast agent for molecular imaging of cancer. *Phys. Med. Biol.* 55(15), 4389–4397 (2010).

68 Kim D, Jeong YY, Jon S. A drug-loaded aptamer–gold nanoparticle bioconjugate for combined CT imaging and therapy of prostate cancer. *ACS Nano* 4(7), 3689–3696 (2010).

69 Reuveni T, Motiei M, Romman Z, Popovtzer A, Popovtzer R. Targeted gold nanoparticles enable molecular CT imaging of cancer: an *in vivo* study. *Int. J. Nanomed.* 6, 2859–2864 (2011).

70 Chattopadhyay N, Cai Z, Kwon YL, Lechtman E, Pignol J-P, Reilly RM. Molecularly targeted gold nanoparticles enhance the radiation response of breast cancer cells and tumor xenografts to x-radiation. *Breast Cancer Res. Treat.* 137(1), 81–91 (2013).

71 Wang H, Zheng L, Peng C, Shen M, Shi X, Zhang G. Folic acid-modified dendrimer-entrapped gold nanoparticles as nanoprobes for targeted CT imaging of human lung adencarcinoma. *Biomaterials* 34(2), 470–480 (2013).

72 Yao L, Daniels J, Moshnikova A *et al.* pHLIP peptide targets nanogold particles to tumors. *Proc. Natl Acad. Sci. USA* 110(2), 465–470 (2013).

73 Ross RD, Roeder RK. Binding affinity of surface functionalized gold nanoparticles to hydroxyapatite. *J. Biomed. Mater. Res.* 99A(1), 58–66 (2011).

74 Lasagna-Reeves C, Gonzalez-Romero D, Barria MA *et al.* Bioaccumulation and toxicity of gold nanoparticles after repeated administration in mice. *Biochem. Biophys. Res. Commun.* 393(4), 649–655 (2010).

75 Pernodet N, Fang X, Sun Y *et al.* Adverse effects of citrate/gold nanoparticles on human dermal fibroblasts. *Small* 2(6), 766–773 (2006).

76 Mironava T, Hadjiargyrou M, Simon M, Jurukovski V, Rafailovich MH. Gold nanoparticles cellular toxicity and recovery: effect of size, concentration and exposure time. *Nanotoxicology* 4(1), 120–137 (2010).

77 Zhang X-D, Wu H-Y, Wu D *et al.* Toxicologic effects of gold nanoparticles *in vivo* by different administration routes. *Int. J. Nanomed.* 5, 771–781 (2010).

78 Cho W-S, Cho M, Jeong J *et al.* Acute toxicity and pharmacokinetics of 13 nm-sized PEG-coated gold nanoparticles. *Toxicol. Appl. Pharm.* 236(1), 16–24 (2009).

79 Cho W-S, Kim S, Han BS, Son WC, Jeong J. Comparison of gene expression profiles in mice liver following intravenous injection of 4 and 100 nm-sized PEG-coated gold nanoparticles. *Toxicol. Lett.* 191(1), 96–102 (2009).

80 Chen Y-S, Hung Y-C, Liau I, Huang GS. Assessment of the *in vivo* toxicity of gold nanoparticles. *Nanoscale Res. Lett.* 4(8), 858–864 (2009).

81 Daniel M-C, Astruc D. Gold nanoparticles: assembly, supramolecular chemistry, quantum-size-related properties, and applications toward biology, catalysis, and nanotechnology. *Chem. Rev.* 104(1), 293–346 (2004).

•• **Detailed review of AuNPs, covering the history, synthesis, surface functionalization and potential applications of AuNPs across many fields.**

82 Link S, El-Sayed MA. Size and temperature dependence of the plasmon absorption of colloidal gold nanoparticles. *J. Phys. Chem. B* 103(21), 4212–4217 (1999).

83 Jain PK, Lee KS, El-Sayed IH, El-Sayed MA. Calculated absorption and scattering properties of gold nanoparticles of different size, shape, and composition: applications in biological imaging and biomedicine. *J. Phys. Chem. B* 110(14), 7238–7248 (2006).

84 Jackson P, Periasamy S, Bansal V, Geso M. Evaluation of the effects of gold nanoparticle shape and size on contrast enhancement in radiological imaging. *Australas. Phys. Eng. Sci. Med.* 34(2), 243–249 (2011).

85 Luo T, Huang P, Gao G *et al.* Mesoporous silica-coated gold nanorods with embedded indocyanine green for dual mode x-ray CT and NIR fluorescence imaging. *Opt. Express* 19(18), 17030–17039 (2011).

86 Lammers T, Aime S, Hennink WE, Storm G, Kiessling F. Theranostic nanomedicine. *Acc. Chem. Res.* 44(10), 1029–1038 (2011).

87 Liu Y, Shipton MK, Ryan J, Kaufman ED, Franzen S, Feldheim DL. Synthesis, stability, and cellular internalization of gold nanoparticles containing mixed peptide–poly(ethylene glycol) monolayers. *Anal. Chem.* 79(6), 2221–2229 (2007).

88 Zhang G, Yang Z, Lu W *et al.* Influence of anchoring ligands and particle size on the colloidal stability and *in vivo* biodistribution of polyethylene glycol-coated gold nanoparticles in tumor-xenografted mice. *Biomaterials* 30(10), 1928–1936 (2009).

89 Ghosh SK, Pal T. Interparticle coupling effect on the surface plasmon resonance of gold nanoparticles: from theory to applications. *Chem. Rev.* 107(11), 4797–4862 (2007).

90 Zhou J, Ralston J, Sedev R, Beattie DA. Functionalized gold nanoparticles: synthesis, structure and colloid stability. *J. Colloid Interf. Sci.* 331(2), 251–262 (2009).

91 Albanese A, Tang PS, Chan WCW. The effect of nanoparticle size, shape, and surface chemistry on biological systems. *Annu. Rev. Biomed. Eng.* 14(1), 1–16 (2012).

92 Sonavane G, Tomoda K, Makino K. Biodistribution of colloidal gold nanoparticles after intravenous administration: effect of particle size. *Colloids Surf. B Biointerfaces* 66(2), 274–280 (2008).

93 De Jong WH, Hagens WI, Krystek P, Burger MC, Sips AJAM, Geertsma RE. Particle size-dependent organ distribution of gold nanoparticles after intravenous administration. *Biomaterials* 29(12), 1912–1919 (2008).

94 Shilo M, Motiei M, Hana P, Popovtzer R. Transport of nanoparticles through the blood–brain barrier for imaging and therapeutic applications. *Nanoscale* 6(4), 2146–2152 (2014).

95 Olivier J-C. Drug transport to brain with targeted nanoparticles. *NeuroRx* 2(1), 108–119 (2005).

96 Niidome T, Yamagata M, Okamoto Y *et al.* PEG-modified gold nanorods with a stealth character for *in vivo* applications. *J. Control. Release* 114(3), 343–347 (2006).

97 Chithrani BD, Chan WCW. Elucidating the mechanism of cellular uptake and removal of protein-coated gold nanoparticles of different sizes and shapes. *Nano Lett.* 7(6), 1542–1550 (2007).

98 Gao H, Shi W, Freud LB. Mechanics of receptor-mediated endocytosis. *Proc. Natl Acad. Sci. USA* 102(27), 9469–9474 (2005).

99 Perrault SD, Walkey C, Jennings T, Fischer HC, Chan WCW. Mediating tumor targeting efficiency of nanoparticles through design. *Nano Lett.* 9(5), 1909–1915 (2009).

100 Pan Y, Neuss S, Leifert A *et al.* Size-dependent cytotoxicity of gold nanoparticles. *Small* 3(11), 1941–1949 (2007).

101 Pan Y, Leifert A, Ruau D *et al.* Gold nanoparticles of diameter 1.4 nm trigger necrosis by oxidative stress and mitochondrial damage. *Small* 5(18), 2067–2076 (2009).

102 Tsoli M, Kuhn H, Brandau W, Esche H, Schmid G. Cellular uptake and toxicity of Au55 clusters. *Small* 1(8–9), 841–844 (2005).

103 Prasad BLV, Stoeva SI, Sorensen CM, Klabunde KJ. Digestive-ripening agents for gold nanoparticles: alternatives to thiols. *Chem. Mater.* 15(4), 935–942 (2003).

104 Giersig M, Mulvaney P. Preparation of ordered colloid monolayers by electrophoretic deposition. *Langmuir* 9(12), 3408–3413 (1993).

105 Brust M, Walker M, Bethell D, Schiffrin DJ, Whyman R. Synthesis of thiol-derivatised gold nanoparticles in a two-phase liquid–liquid system. *J. Chem. Soc. Chem. Commun.* 7, 801–802 (1994).

106 Brust M, Fink J, Bethell D, Schiffrin DJ, Kiely C. Synthesis and reactions of functionalised gold nanoparticles. *J. Chem. Soc. Chem. Comm.* 16, 1655–1656 (1995).

107 Leff DV, Brandt L, Heath JR. Synthesis and characterization of hydrophobic, organically-soluble gold nanocrystals functionalized with primary amines. *Langmuir* 12(20), 4723–4730 (1996).

108 Aslam M, Fu L, Su M, Vijayamohanan K, Dravid VP. Novel one-step synthesis of amine-stabilized aqueous colloidal gold nanoparticles. *J. Mater. Chem.* 14(12), 17951797 (2004).

109 Brown LO, Hutchison JE. Formation and electron diffraction studies of ordered 2-D and 3-D superlattices of amine-stabilized gold nanocrystals. *J. Phys. Chem. B* 105(37), 8911–8916 (2001).

110 Porter LA, Ji D, Westcott SL *et al.* Gold and silver nanoparticles functionalized by the adsorption of dialkyl disulfides. *Langmuir* 14(26), 7378–7386 (1998).

111 Yonezawa T, Yasui K, Kimizuka N. Controlled formation of smaller gold nanoparticles by the use of four-chained disulfide stabilizer. *Langmuir* 17(2), 271–273 (2001).

112 Yao H, Momozawa O, Hamatani T, Kimura K. Stepwise size-selective extraction of carboxylate-modified gold nanoparticles from an aqueous suspension into toluene with tetraoctylammonium cations. *Chem. Mater.* 13(12), 4692–4697 (2001).

113 Weare WW, Reed SM, Warner MG, Hutchison JE. Improved synthesis of small (dcore ≈ 1.5 nm) phosphine-stabilized gold nanoparticles. *J. Am. Chem. Soc.* 122(51), 12890–12891 (2000).

114 Schmid G. Large clusters and colloids. Metals in the embryonic state. *Chem. Rev.* 92(8), 1709–1727 (1992).

115 Selvakannan P, Mandal S, Phadtare S, Pasricha R, Sastry M. Capping of gold nanoparticles by the amino acid lysine renders them water-dispersible. *Langmuir* 19(8), 3545–3549 (2003).

116 Love JC, Estroff LA, Kriebel JK, Nuzzo RG, Whitesides GM. Self-assembled monolayers of thiolates on metals as a form of nanotechnology. *Chem. Rev.* 105(4), 1103–1170 (2005).

117 Yang M, Yau HC, Chan HL. Adsorption kinetics and ligand-binding properties of thiol-modified double-stranded DNA on a gold surface. *Langmuir* 14(21), 6121–6129 (1998).

118 Esumi K, Suzuki A, Aihara N, Usui K, Torigoe K. Preparation of gold colloids with UV irradiation using dendrimers as stabilizer. *Langmuir* 14(12), 3157–3159 (1998).

119 Garcia ME, Baker LA, Crooks RM. Preparation and characterization of dendrimer–gold colloid nanocomposites. *Anal. Chem.* 71(1), 256–258 (1999).

120 Esumi K, Suzuki A, Yamahira A, Torigoe K. Role of poly(amidoamine) dendrimers for preparing nanoparticles of gold, platinum, and silver. *Langmuir* 16(6), 2604–2608 (2000).

121 Shi X, Wang S, Sun H, Baker JR. Improved biocompatibility of surface functionalized dendrimer-entrapped gold nanoparticles. *Soft Matter* 3(1), 71–74 (2007).

122 Shi X, Wang S, Meshinchi S *et al.* Dendrimer-entrapped gold nanoparticles as a platform for cancer-cell targeting and imaging. *Small* 3(7), 1245–1252 (2007).

123 Liu H, Xu Y, Wen S *et al.* Targeted tumor computed tomography imaging using low-generation dendrimer-stabilized gold nanoparticles. *Chem. Eur. J.* 19(20), 6409–6416 (2013).

124 Wang H, Zheng L, Peng C *et al.* Computed tomography imaging of cancer cells using acetylated dendrimer-entrapped gold nanoparticles. *Biomaterials* 32(11), 2979–2988 (2011).

125 Chen Q, Li K, Wen S *et al.* Targeted CT/MR dual model imaging of tumors using multifunctional dendrimer-entrapped gold nanoparticles. *Biomaterials* 34(21), 5200–5209 (2013).

126 Tomalia DA. Dendrons/dendrimers: quantized, nano-element like building blocks for soft-soft and soft–hard nano-compound synthesis. *Soft Matter* 6(3), 456–747 (2010).

127 Sperling RA, Rivera Gil P, Zhang F, Zanella M, Parak WJ. Biological applications of gold nanoparticles. *Chem. Soc. Rev.* 37(9), 1896–1908 (2008).

128 Kattumuri V, Katti K, Bhaskaran S *et al.* Gum arabic as a phytochemical construct for the stabilization of gold nanoparticles: *in vivo* pharmacokinetics and x-ray–contrast-imaging studies. *Small* 3(2), 333–341 (2007).

129 Ross RD, Cole LE, Roeder RK. Relative binding affinity of carboxylate-, phosphonate-, and bisphosphonate-functionalized gold nanoparticles targeted to damaged bone tissue. *J. Nanopart. Res.* 14(10), 1175 (2012).

130 Cole LE, Vargo-Gogola T, Roeder RK. Bisphosphonate-functionalized gold nanoparticles for contrast-enhanced x-ray detection of breast microcalcifications. *Biomaterials* 35(7), 2312–2321 (2014).

131 Zhang Z, Ross RD, Roeder RK. Preparation of functionalized gold nanoparticles as a targeted x-ray contrast agent for damaged bone tissue. *Nanoscale* 2(4), 582–586 (2010).

132 Allijn IE, Leong W, Tang J *et al.* Gold nanocrystal labeling allows low-density lipoprotein imaging from the subcellular to macroscopic level. *ACS Nano* 7(11), 9761–9770 (2013).

133 Choi CHJ, Alabi CA, Webster P, Davis ME. Mechanism of active targeting in solid tumors with transferrin-containing gold nanoparticles. *Proc. Natl Acad. Sci. USA* 107(3), 1235–1240 (2010).

134 Zhou J, Beattie DA, Ralston J, Sedev R. Colloid stability of thymine-functionalized gold nanoparticles. *Langmuir* 23(24), 12096–12103 (2007).

135 Otsuka H, Nagasaki Y, Kataoka K. PEGylated nanoparticles for biological and pharmaceutical applications. *Adv. Drug Deliv.. Rev.* 55(3), 403–419 (2003).

136 Hayashi K, Nakamura M, Miki H *et al.* Gold nanoparticle cluster-plasmon-enhanced fluorescent silica core–shell nanoparticles for x-ray computed tomography–fluorescence dual-mode imaging of tumors. *Chem. Commun.* 49(46), 5334 (2013).

137 Kah JCY, Wong KY, Neoh KG *et al.* Critical parameters in the PEGylation of gold nanoshells for biomedical applications: an *in vitro* macrophage study. *J. Drug Target.* 17(3), 181–193 (2009).

138 Cho W-S, Cho M, Jeong J *et al.* Size-dependent tissue kinetics of PEG-coated gold nanoparticles. *Toxicol. Appl. Pharm.* 245(1), 116–123 (2010).

139 Chattopadhyay N, Fonge H, Cai Z *et al.* Role of antibody-mediated tumor targeting and route of administration in nanoparticle tumor accumulation *in vivo*. *Mol. Pharm.* 9(8), 2168–2179 (2012).